

AD-A189 234

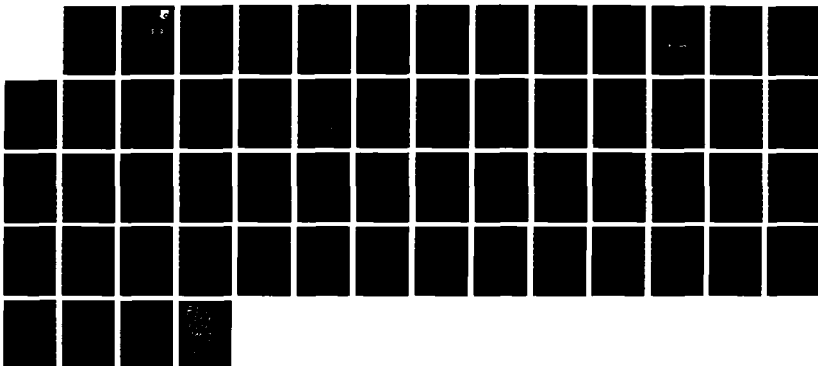
SOAR: SPACE ORBITING ADVANCED FUSION POWER REACTOR(U)
WISCONSIN UNIV-MADISON F L KULCINSKI ET AL. SEP 87
AFMNL-TR-87-2048 F33615-86-C-2705

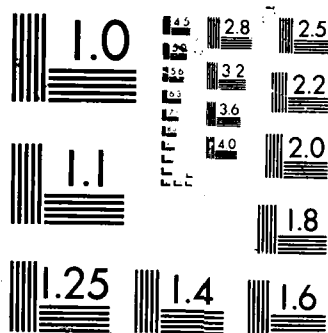
1/1

UNCLASSIFIED

F/G 22/2

NL





AFWAL-TR-87-2048

DTIC FILE COPY

SOAR: SPACE ORBITING ADVANCED FUSION POWER REACTOR



F. L. Kulcinski
J. F. Santarius

UNIVERSITY OF WISCONSIN
1500 JOHNSON DRIVE
MADISON, WISCONSIN 53706-1687

DTIC
ELECTE
DEC 10 1987
S D

SEPTEMBER 1987

FINAL REPORT FOR PERIOD OCTOBER 1986 - JANUARY 1987

APPROVED FOR PUBLIC RELEASE; DISTRIBUTION IS UNLIMITED.

AERO PROPULSION LABORATORY
AIR FORCE WRIGHT AERONAUTICAL LABORATORIES
AIR FORCE SYSTEMS COMMAND
WRIGHT PATTERSON AIR FORCE BASE, OHIO 45433-6563

NOTICE

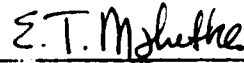
When Government drawings, specifications, or other data are used for any purpose other than in connection with a definitely related Government procurement operation, the United States Government thereby incurs no responsibility nor any obligation whatsoever; and the fact that the government may have formulated, furnished, or in any way supplied the said drawings, specifications, or other data, is not to be regarded by implication or otherwise as in any manner licensing the holder or any other person or corporation, or conveying any rights or permission to manufacture use, or sell any patented invention that may in any way be related thereto.

This report has been reviewed by the Office of Public Affairs (ASD/PA) and is releasable to the National Technical Information Service (NTIS). At NTIS, it will be available to the general public, including foreign nations.

This technical report has been reviewed and is approved for publication.

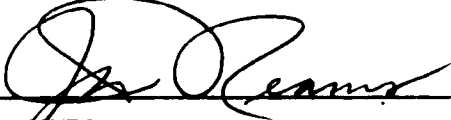


ELLIOT B. KENNEL
Project Engineer



EDWARD T. MAHEFKEY, TAM
Nuclear Thermal Systems Group
Power Technology Branch

FOR THE COMMANDER



JAMES D. REAMS
Chief, Aerospace Power Division
Aero Propulsion Laboratory

If your address has changed, if you wish to be removed from our mailing list, or if the addressee is no longer employed by your organization please notify AFWAL/POOS-3 W-PAFB, OH 45433 to help us maintain a current mailing list.

Copies of this report should not be returned unless return is required by security considerations, contractual obligations, or notice on a specific document.

UNCLASSIFIED

SECURITY CLASSIFICATION OF THIS PAGE

REPORT DOCUMENTATION PAGE				Form Approved OMB No. 0704-0188	
1a. REPORT SECURITY CLASSIFICATION Unclassified			1b. RESTRICTIVE MARKINGS None		
2a. SECURITY CLASSIFICATION AUTHORITY N/A			3. DISTRIBUTION/AVAILABILITY OF REPORT Approved for public release; distribution unlimited		
2b. DECLASSIFICATION/DOWNGRADING SCHEDULE N/A					
4. PERFORMING ORGANIZATION REPORT NUMBER(S)			5. MONITORING ORGANIZATION REPORT NUMBER(S) AFWAL-TR-87-2048		
6a. NAME OF PERFORMING ORGANIZATION University of Wisconsin		6b. OFFICE SYMBOL (If applicable)	7a. NAME OF MONITORING ORGANIZATION Air Force Wright Aeronautical Laboratories Aero Propulsior. Laboratory (AFWAL/POOS-3)		
6c. ADDRESS (City, State, and ZIP Code) 1500 Johnson Dr Madison, Wisc 5306-1687			7b. ADDRESS (City, State, and ZIP Code) WPAFB, OH 45433-6563		
8a. NAME OF FUNDING/SPONSORING ORGANIZATION SDIO		8b. OFFICE SYMBOL (If applicable) 1st	9. PROCUREMENT INSTRUMENT IDENTIFICATION NUMBER F33615-86-C-2705		
8c. ADDRESS (City, State, and ZIP Code) The Pentagon Washington, DC 20301-7100			10. SOURCE OF FUNDING NUMBERS		
			PROGRAM ELEMENT NO. 1	PROJECT NO. 0281	TASK NO. 20
11. TITLE (Include Security Classification) SOAR: Space Orbiting Advanced Fusion Power Reactor					
12. PERSONAL AUTHOR(S) G. L. Kulcinski					
13a. TYPE OF REPORT (Final)		13b. TIME COVERED FROM 10-86 TO 1-87	14. DATE OF REPORT (Year, Month, Day) September 1987		15. PAGE COUNT 59
16. SUPPLEMENTARY NOTATION					
17. COSATI CODES			18. SUBJECT TERMS (Continue on reverse if necessary and identify by block number) I. Fusion Power II. Spacecraft thermal management		
FIELD	GROUP	SUB-GROUP			
22	02				
19. ABSTRACT (Continue on reverse if necessary and identify by block number) (See Reverse)					
20. DISTRIBUTION/AVAILABILITY OF ABSTRACT <input checked="" type="checkbox"/> UNCLASSIFIED/UNLIMITED <input type="checkbox"/> SAME AS RPT <input type="checkbox"/> DTIC USERS			21. ABSTRACT SECURITY CLASSIFICATION Unclassified		
22a. NAME OF RESPONSIBLE INDIVIDUAL Elliot B Kennel			22b. TELEPHONE (Include Area Code) 513-255-6241		22c. OFFICE SYMBOL AFWAL/POOS-3

BLOCK 19

This is the final report of Air Force Contract F33615-86-C-2705. The preconceptual design of a Space Orbiting Advanced Fusion Power Reactor (SOAR), which delivers up to 1000 MWe for at least 600 s from an orbited mass of about 500 tonnes, has been accomplished. The power is produced by a magnetically confined $D-^3He$ plasma. Approximately 96% of the fusion energy is in charged particles, and a direct converter has been designed which converts much of this energy into electricity at high net efficiency ($\sim 80\%$). An advanced shield design allows SOAR to deliver approximately 2 kilowatts of electricity for every kilogram of material orbited. The shield is designed to absorb all rejected heat during operation, and no active radiator is required. The SOAR reactor concept is designed to allow rapid startup and shutdown procedures. The lack of radioactivity on launch and the low radioactive inventory after operation make the SOAR concept attractive from maintenance, safety and environmental perspectives. The plasma physics approach extrapolates from the present plasma physics and fusion technology knowledge base using concepts which can be tested on existing or near-term devices. The symbiosis of burst mode requirements, $D-^3He$ tandem mirror fusion reactor characteristics, and the space environment leads to a very high performance design concept.

Three papers relating to the SOAR study were presented at the Symposium on Space Nuclear Power Systems at Albuquerque, New Mexico, on January 12-16, 1987. These were: an overview paper titled "SOAR: Space Orbiting Advanced Fusion Power Reactor" (Santarius et al. 1987a); a paper on shielding titled "Magnet Shielding Analysis for SOAR -- A Space Reactor" (El-Guebaly 1987); and "Helium-3 Fusion Fuel Resources for Space Power" (Wittenberg et al. 1987). This progress report contains most of the material from those papers, supplemented by other, related work we have accomplished under this contract.

TABLE OF CONTNETS

SECTION		PAGE
I	Introduction	1
II	Plasma Physics and Engineering	2
III	Magnetics and Cryogenics	12
IV	Magnet Shielding	20
V	Heat Dissipation in the SOAR Reactor	31
VI	Direct Converter	37
VII	Power Handling	46
	References	49

Accession For	
NTIC GRA&I	<input checked="" type="checkbox"/>
DTIC TAB	<input type="checkbox"/>
Unannounced	<input type="checkbox"/>
Justification	
By	
Date	
Approved for Release	
Class	Excluded from automatic downgrading and declassification
A-1	



LIST OF ILLUSTRATIONS

FIGURE	PAGE
1. General Configuration of 250 MWe and 1000 MWe Versions of SOAR. The Space Shuttle is Shown for Comparison.	3
2. The Three Main Fusion Reactions and Their Reactivities.	4
3. Percentage of Fusion Reaction Energy in Charged Particles for an Assumed Tritium Burn Fraction of 50%.	5
4. Axial Dependence of Magnetic Field Magnitude, Electrostatic Potential, and Densities for SOAR.	9
5. Progress of Tandem Mirror Reactor Conceptual Designs Toward Axisymmetry and Simpler Systems.	11
6. Simplified Plasma Power Balance.	13
7. SOAR Plant Power Balance.	14
8. Isometric View of the SOAR Magnet Winding Pack Envelopes.	15
9. Schematic of Central Cell Shield and Superconducting Magnet.	25
10. Variation of the Nuclear Heating in the Magnet with the Thickness of the Different Shields for SOAR-250.	29
11. Mass of Central Cell Components as a Function of the Shield Thickness for SOAR-250.	30
12. Mass of Central Cell Components as a Function of the LiH Shield Thickness for SOAR-1000.	32
13. A Section of the Central Cell with the Plasma in the Center, Surrounded by the Shield and the Magnet. Arrows Show the Flow Distribution of the He Gas.	35
14. Average Temperature of the SOAR Shield as a Function of Time.	36
15. Effect of Temperature on the Yield Strength of Several Candidate Materials.	38
16. Ratio of Thermal Stress to Yield Strength for Selected Candidate Materials.	39
17. Schematic of a 2-Stage Direct Converter.	41

LIST OF TABLES

TABLE	PAGE
1. Key Parameters for SOAR.	6
2. Terrestrial Resources of ^3He .	7
3. Preliminary SOAR Plasma Parameters.	16
4. Preliminary SOAR Reference Case Magnet Parameters.	17
5. Materials Evaluated for the Shield.	23
6. Neutronics-Related Parameters for the 250 and 1000 MWe Designs of SOAR.	26
7. Effect of Shielding, Structural, Coolant Materials on Peak Nuclear Heating in the S/C Magnets.	27
8. Comparison between the Masses of the Central Cell Components for the Four Shields.	33
9. Pertinent Properties of LiH and Li for the Shield Adiabatic Heatup Calculations.	34
10. Energy Spectrum Entering the Direct Converter.	42
11. The Six Direct Converter Suppressor Grid Cooling Concepts and Their Masses.	44
12. Suppressor Grid Diameter and Mass for the Three Grid Materials Radiating between 1400 and 2000 C.	44
13. Masses of the Grids, Collectors, and Structural Supports for the Ion End Direct Converter of SOAR.	46

I. INTRODUCTION

Fusion reactors based on the deuterium/helium-3 ($D-^3\text{He}$) reaction are efficient for space burst mode power because:

- Sufficient terrestrial ^3He reserves exist for the near-term use of "low-neutron" $D-^3\text{He}$ fuel;
- The radiation shielding mass is reduced;
- Radiators can be eliminated by dissipating waste heat adiabatically in the shield during full power operation;
- Highly efficient direct electrostatic conversion of energy to electricity by the use of low mass direct converters is possible;
- Vacuum pumping equipment is eliminated and cryogenic cooling systems are reduced in mass and complexity;
- The SOAR reactor is nonradioactive until operated;
- No "criticality" potential exists during a launch phase accident;
- Low radioactivity and afterheat levels are induced during operation and only short half life isotopes remain for waste disposal; and
- Response from a cold start can be rapid (~ 10 seconds).

Many of these advantages had been identified previously, and $D-^3\text{He}$ fusion reactors for use in space (Englert 1962, Hilton et al. 1964) and on Earth (Miley 1976, Dawson 1981, Santarius 1987b) have been under investigation for some time.

Our calculations indicate that a tandem mirror magnetic confinement device would make the most efficient use of this advanced fuel. The main reasons for this are the possibility of electrostatic direct conversion and the ease of increasing magnetic fields to maintain plasma pressure. The general configuration for the 250 MWe and 1000 MWe versions of SOAR is indicated

in Figure 1, where the Space Shuttle is also shown for comparison. Other concepts such as toroidal fusion reactors or inertial confinement (laser or ion beam driven) fusion reactors have been considered, but preliminary estimates of the mass utilization favor the tandem mirror.

At this time, the SOAR study is primarily aimed at critical issues and, due to resource and time limitations, not all of the details of the design are self-consistent. The intent of this phase of the SOAR study was to identify areas requiring more intense work and to estimate masses sufficient for a preliminary assessment of the attainable power to mass ratio at a given power level. A nominal reference case, based on a power level of 1000 MWe and a 600 s operation time, has also been generated in order to define characteristic parameters. Some key parameters are given in Table 1.

II. PLASMA PHYSICS AND ENGINEERING

The key advantage that a $D-^3He$ fusion reactor has over both fission reactors and deuterium/tritium (D/T)-fueled fusion reactors is that almost all of the energy generated by the nuclear reactions is in the form of charged particles. Besides reducing the mass required for neutron shielding, this potentially allows direct electrostatic conversion of charged particle energy to electricity at efficiencies much higher than attainable through a Carnot cycle. The three main fusion reactions and their reactivities are shown in Figure 2. The percentage of fusion reaction energy in charged particles for each of these reactions is shown in Figure 3. For typical SOAR parameters, less than 4% of the fusion energy is carried by neutrons. The generic advantage of reduced neutron shielding requirements applies to any magnetic con-

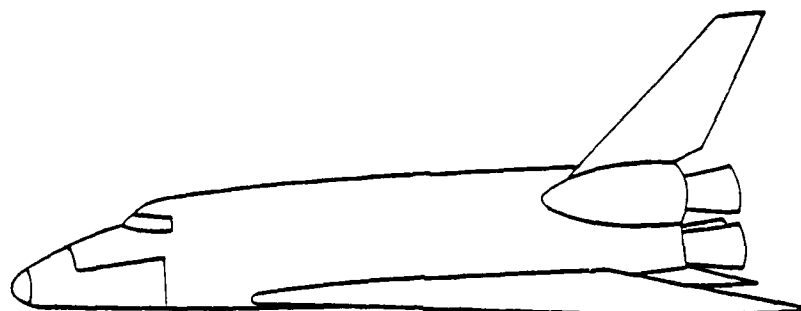


FIGURE 1. General Configuration of 250 MWe and 1000 MWe Versions of SOAR.
The Space Shuttle is Shown for Comparison.

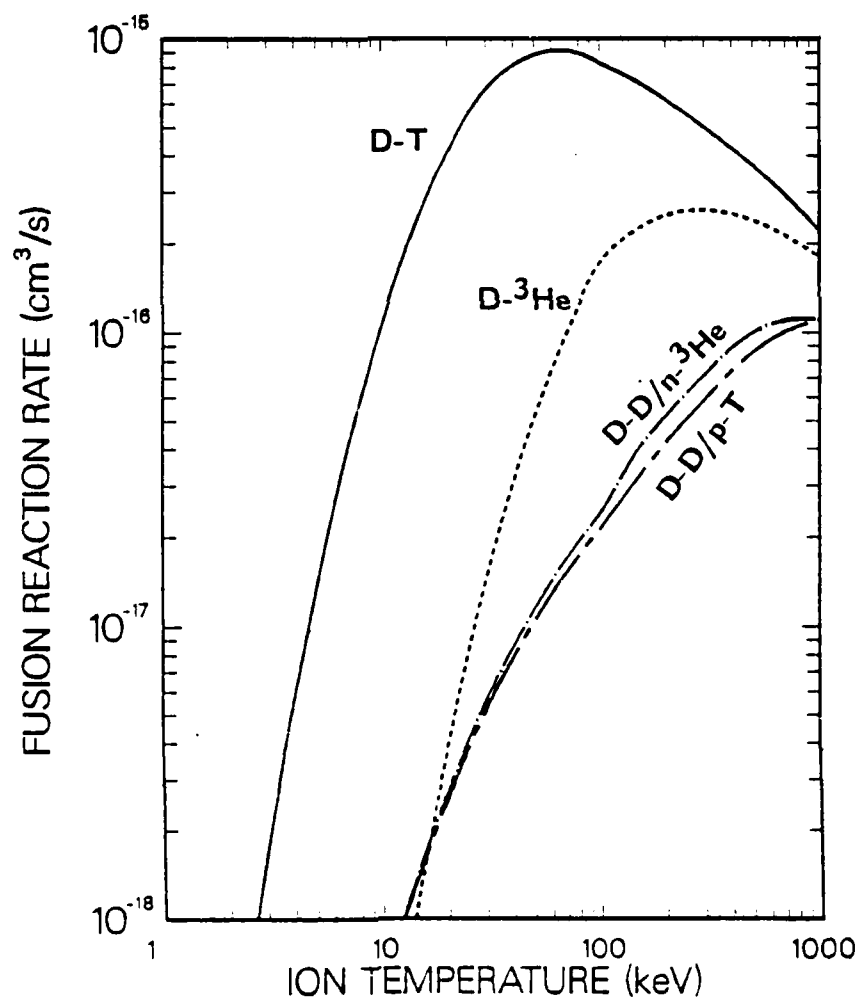
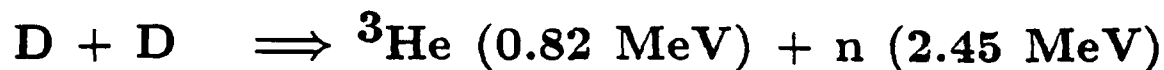
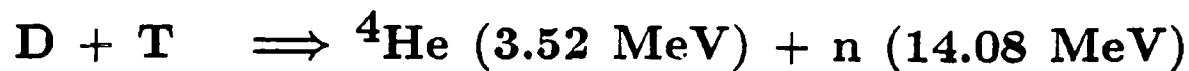
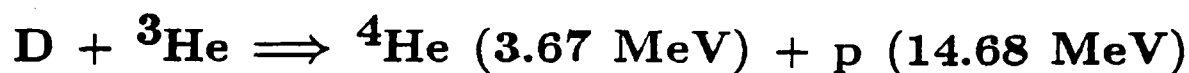


FIGURE 2. The Three Main Fusion Reactions and Their Reactivities.

PERCENT OF FUSION POWER IN NEUTRONS (50% Tritium Burnup)

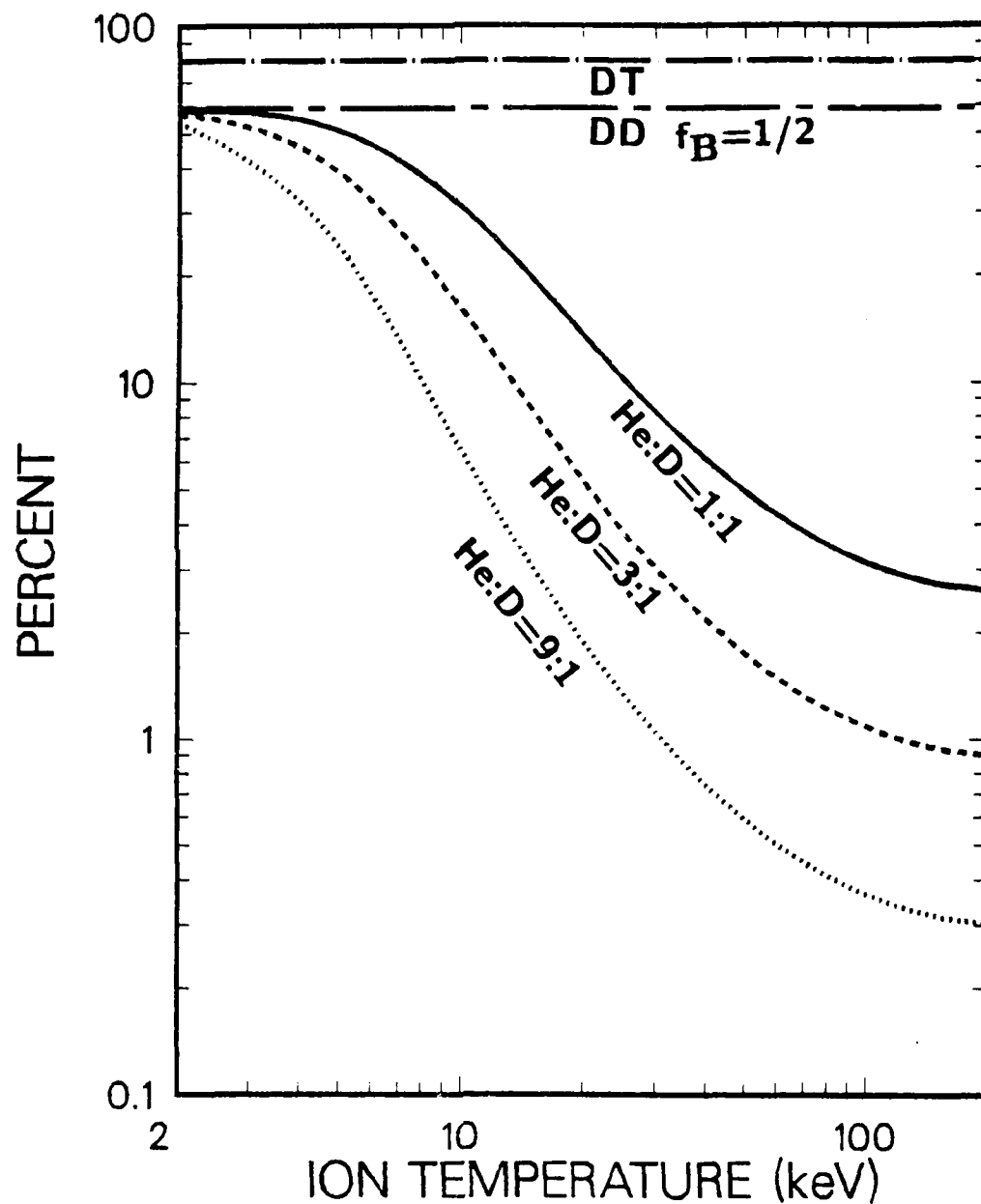


FIGURE 3. Percentage of Fusion Reaction Energy in Charged Particles.

TABLE 1. Key Parameters for SOAR

Mass utilization	~ 2 kWe/kg
Net efficiency	53%
Net power	1000 MWe
Recirculating power	10%
Total mass	~ 500 tonnes
Fusion power	1900 MW
Operation time	600 s
Central cell first wall radius	0.63 m
First wall surface heat load	1.6 MW/m ²
Shield thickness	0.36 m
Energy dissipated in shield	342 GJ
Initial shield temperature	200 K
Final average shield temperature	808 K

finement concept, but direct conversion is most readily utilized in an open field line geometry. Therefore, the tandem mirror configuration has been chosen for the initial SOAR reference case.

Terrestrial fusion power reactor designs based on the $^3\text{He}(d,p)\alpha$ reaction have been less intensely studied than those based on the $t(d,n)\alpha$, $d(d,n)^3\text{He}$, and $d(d,p)t$ reactions due to the scarcity of ^3He on Earth. However, sufficient ^3He for a 1000 MWe SOAR reactor, operating for 10 minutes, would be only 10 g and cost ~ \$7000 (Wittenberg et al. 1986). The potential terrestrial resources of ^3He have been surveyed and are given in Table 2 (Wittenberg et al., 1987). The readily accessible, naturally occurring resources are principally limited to those in the natural gas wells. A large reservoir, 4×10^6 kg

TABLE 2. Terrestrial Resources of ^3He

Source	Helium Content (vol. ratio $\times 10^{-6}$)	$^3\text{He}/^4\text{He}$ (at. ratio $\times 10^{-6}$)	^3He Content (kg)	Equivalent ^(a) MWe-(yr)
<u>NATURAL</u>				
U.S. Natural Gas Wells				
Present Storage	10^6	0.2	29	290
Known Reserves	3×10^3	0.2	187	1870
<u>MAN-MADE</u>				
U.S. DOE				
MRC Sales			1.3/yr	
MRC Inventory			13.4	
CANDU Reactors (by year 2000)				
Production			2/yr	
Inventory			10	
Weapons Stockpile ^(b)			15/yr	
			18	180
	TOTAL	ANNUAL ----- INVENTORY	----- 239	----- 2390
(a) 10 MWe-yr/kg - ^3He				
(b) Estimate (Wittenberg et al., 1986)				

of ^3He , exists in the atmosphere; however, helium is highly stratified in the atmosphere, mostly concentrated in the stratosphere, and no economic recovery method is apparent. The man-made ^3He sources, due to the decay of tritium, are currently used for a variety of research projects. The USDOE-Monsanto Research Corp. currently sells up to 1.3 kg/yr and has a 13 kg inventory. The Canadian CANDU reactors produce tritium in their D_2O moderators. By 1987,

Ontario Hydro will begin to separate and store this tritium. Due to the decay of tritium at least 10 kg of ^3He should be available by the year 2000 and, thereafter, it will be produced at ~ 2 kg/yr. The decay of tritium from stored thermonuclear weapons in the world represents a significant source of ^3He , if it could be made available. For instance, unclassified estimates of the U.S. Strategic Forces inventory indicate that ~ 15 kg/yr of ^3He could be expected. In summary, as shown in Table 2, the total of all the known sources of ^3He indicates that several 100 MWe power plants could be operated continuously for research and development purposes.

A tandem mirror fusion reactor is essentially a linear magnetic bottle in which plasma end loss is reduced by a combination of magnetic fields ("magnetic mirrors") and electrostatic potentials (Baldwin and Logan 1979, Kesner et al. 1984, and Logan et al. 1986). The axial profiles of magnetic field, potential, and the various plasma species for SOAR are shown in Figure 4. The thermal barrier region serves to thermally insulate the central cell from the plug region. This allows ion end loss to be reduced through a linear dependence of the plug electrostatic potential on electron temperature rather than through a logarithmic dependence on density. The governing relation is approximately:

$$\phi_i + \phi_b = T_{ep} \ln \left[\left(\frac{T_{ec}}{T_{ep}} \right)^{1/2} \frac{n_p}{n_b - n_{eh}} \right] \quad (1)$$

where ϕ_i is the ion-confining potential, ϕ_b is the thermal barrier potential, T_{ec} is the central cell electron temperature, T_{ep} is the plug electron temperature, n_p is the total plug density, n_b is the total barrier density, and n_{eh}

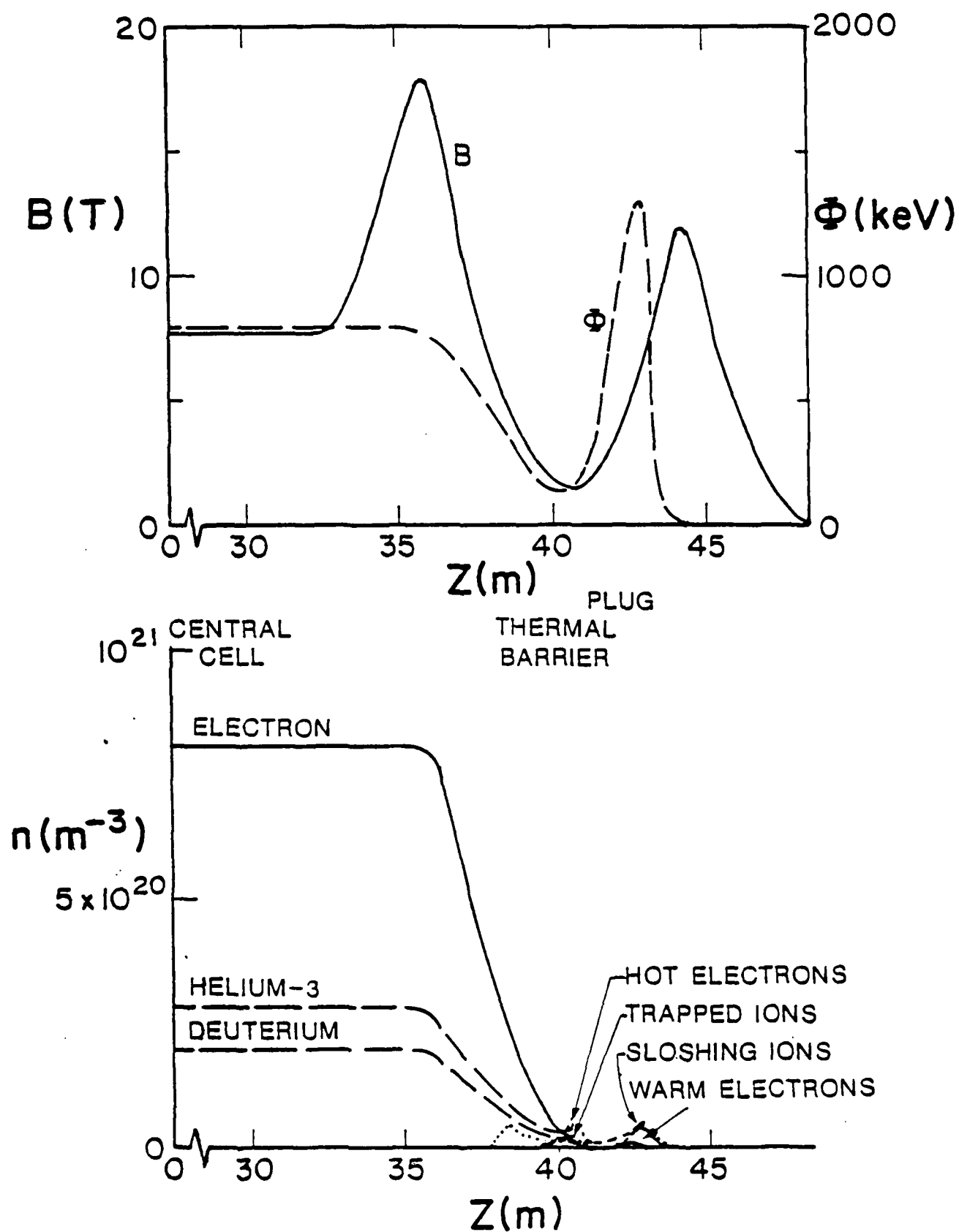


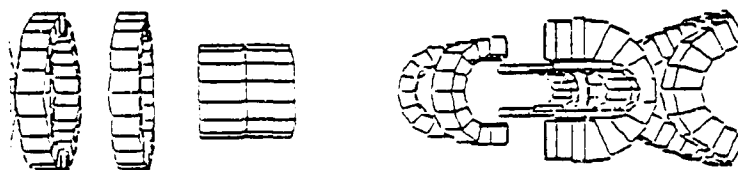
FIGURE 4. Axial Dependence of Magnetic Field Magnitude, Electrostatic Potential, and Densities for SOAR.

is the hot electron density in the thermal barrier. The potentials are maintained by creating non-Maxwellian (nonequilibrium) populations of ions via neutral beam (NB) injection and of electrons via electron cyclotron range of frequencies (ECRF) heating. The fusion power is produced in the central cell region by nearly Maxwellian populations of deuterium and helium-3 ions. The core plasma is surrounded by a low density, low temperature halo plasma which pumps away impurities due to wall outgassing or other neutral gas sources.

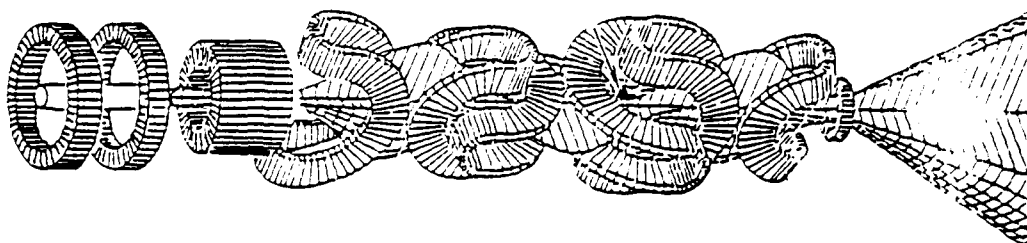
Stable, axisymmetric operation is assumed to be maintained in SOAR by allotting 25 MW of absorbed power to central cell ion cyclotron range of frequencies (ICRF) heating. This invokes so-called RF stabilization (Hershkowitz et al. 1985). Two other attractive candidate methods of achieving axisymmetry are presently under investigation: wall stabilization (Berk et al. 1984), and magnetic limiter stabilization (Kesner et al. 1985). These would eliminate the requirement for central cell ICRF power and we have deliberately chosen the more conservative option at this time. Although a substantial theoretical and experimental effort on these topics is in progress in the fusion community, the critical issues involved will require high power and high density experiments for their resolution. The trend toward axisymmetry and simpler systems is illustrated in Figure 5, which schematically shows the configurations of recent tandem mirror reactor studies.

The SOAR plasma is modeled using standard thermal barrier tandem mirror reactor theory (Logan et al. 1984 and 1986), suitably modified for the D-³He fuel cycle. In addition, a new operating mode is examined -- in which the fusion product protons not needed to sustain plasma losses are caused to scatter quickly (nonadiabatically) and to be lost out the ends on a time scale

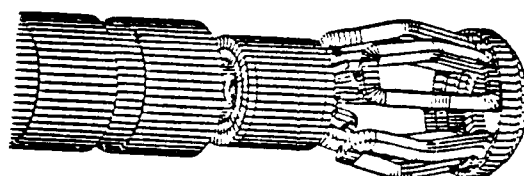
WITAMIR-I
1980



MARS
1984



MINIMARS
1986



SOAR
1987

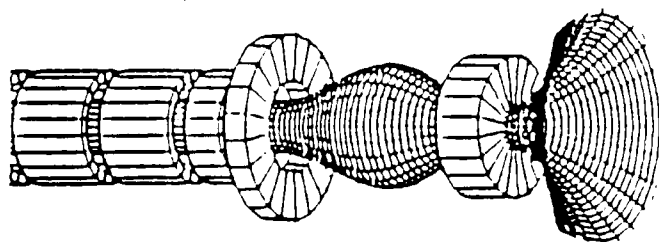


FIGURE 5. Progress of Tandem Mirror Reactor Designs Conceptual Toward Axisymmetry and Simpler Systems.

short compared to the time it would take them to deposit their energy in the core plasma (Santarius 1987b). The resulting, narrow energy spectrum of the proton end loss stream should lead to a high direct converter (all input species) efficiency ($> 80\%$). This new mode is a desirable, but not necessary, feature of a D- ^3He tandem mirror reactor design. The option of allowing the fusion products to slow down in the core plasma is still under investigation; this would mitigate the difficulties of designing a high voltage direct converter. A tandem mirror reactor computer code, PBSOAR, has been written to solve the particle and power balance equations involved and to assess the performance of SOAR. Using simple mass scaling laws generated in the course of this study for the most important components of SOAR, the reactor parameters were optimized for power per mass over a space of 21 variables. Reference case plasma physics parameters for a 1000 MWe version of SOAR are given in Table 3. A simplified plasma power flow chart is shown in Figure 6, while the plant power flow is given in Figure 7.

III. MAGNETICS AND CRYOGENICS

The 1000 MWe reference case has a central cell, on-axis field of 7.7 T, 18 T choke coils at each end of the central cell, and 12 T end coils outside of the choke coils. The parameters for the magnet system are given in Table 4; an isometric view of the winding pack envelopes is given in Figure 8. All coils in the system are axisymmetric solenoids.

Choice of Central Cell Magnet Technology

The nominal SOAR operating scenario is a single 600 s burn. Use of both resistive (liquid hydrogen-cooled aluminum) and superconducting windings was

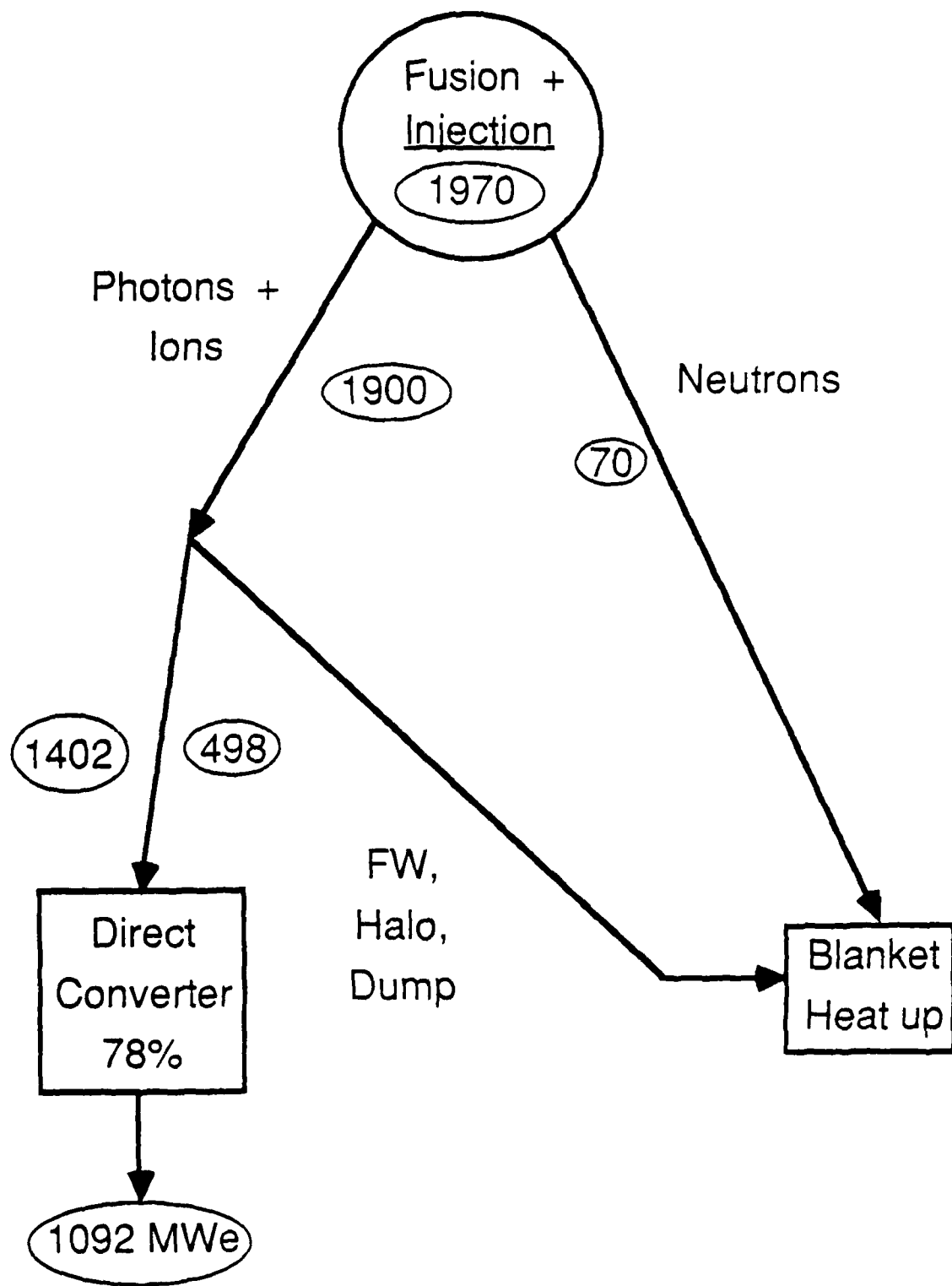


FIGURE 6. Simplified Plasma Power Balance.

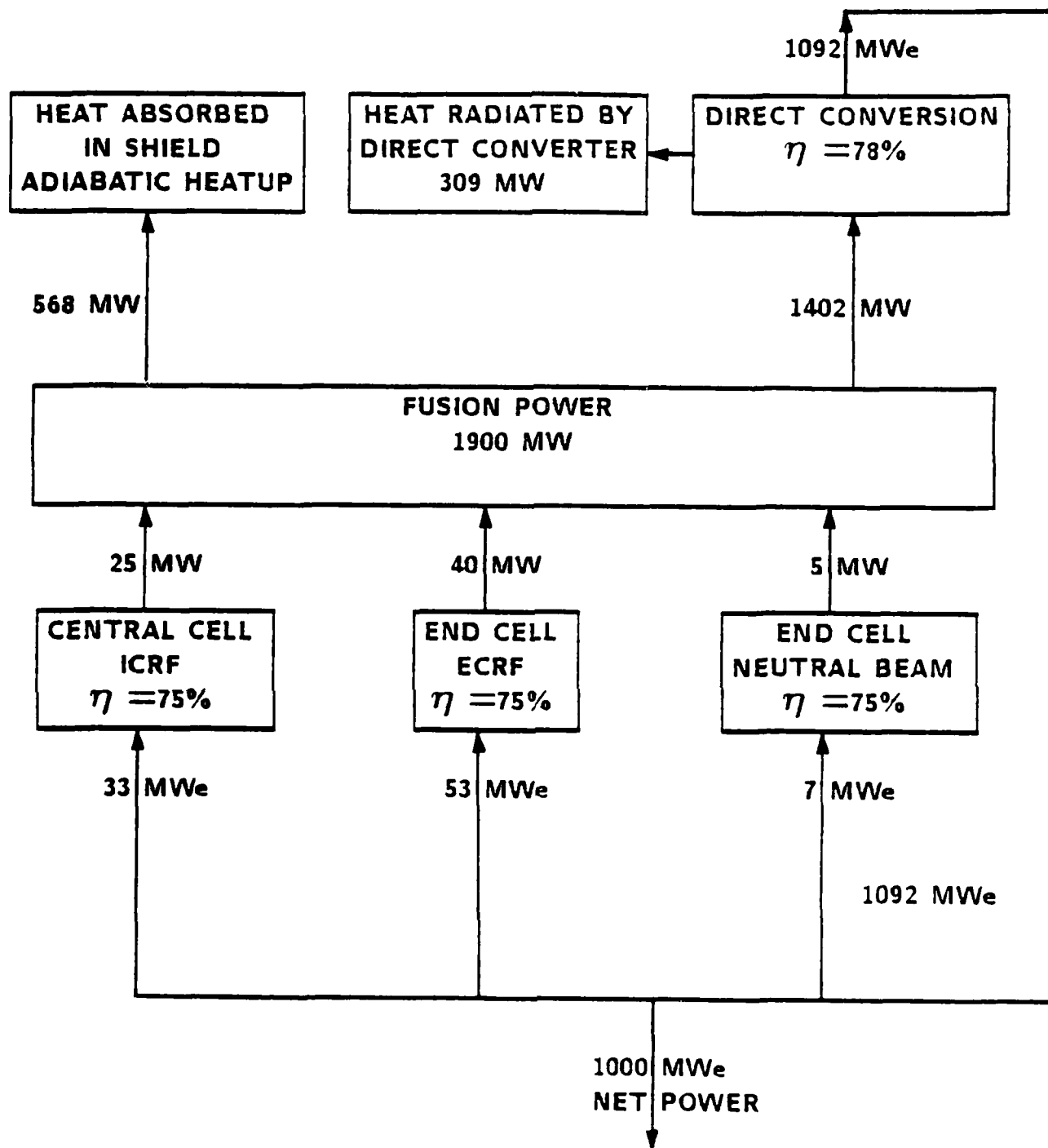


FIGURE 7. SOAR Plant Power Balance.

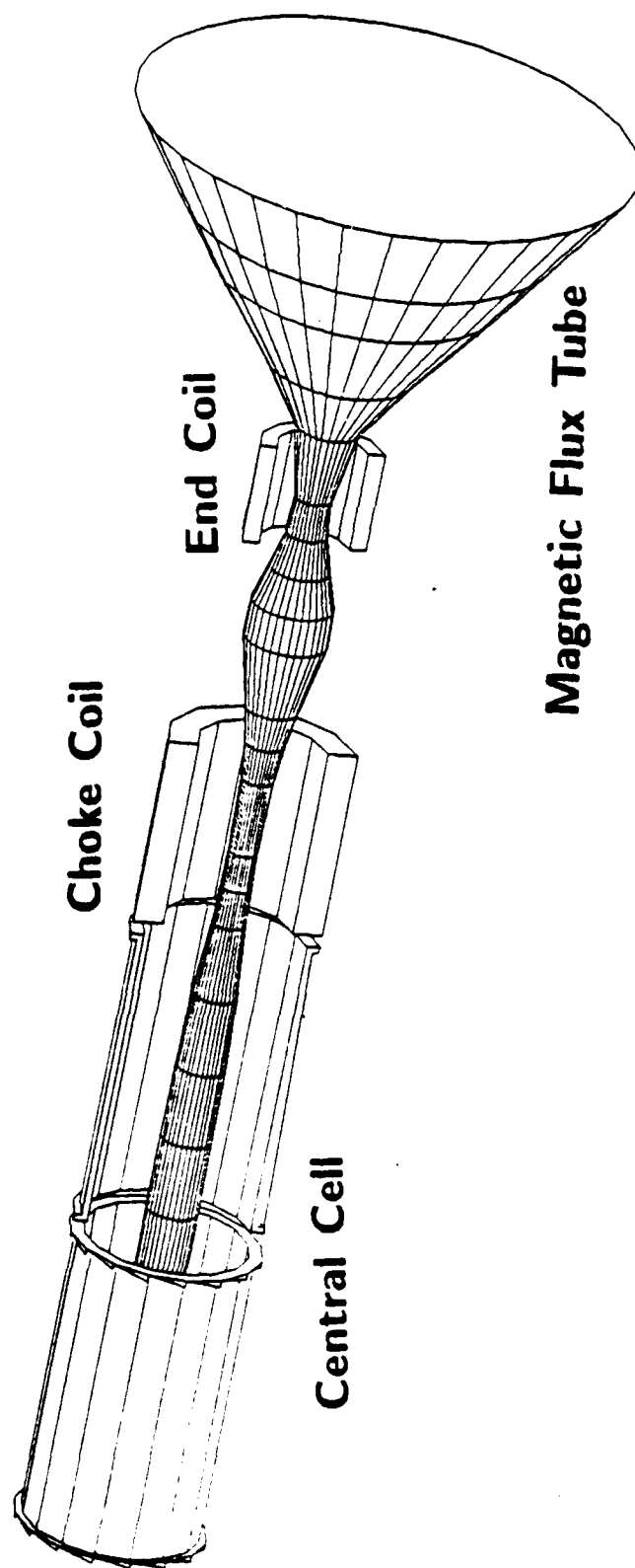


FIGURE 8. Isometric View of the SOAR Magnet Winding Pack Envelopes.

TABLE 3. Preliminary SOAR Plasma Parameters

Fusion power	1900 MW
Percent of fusion power in nonadiabatic protons	53%
Percent of fusion power in neutrons	3.6%
Central cell ICRF heating power	25 MW
End cell heating power	45 MW
Bremsstrahlung and synchrotron radiation	470 MW
Central cell (power producing region)	
³ He to D density ratio	1.4
Plasma radius	0.55 m
Length	73 m
On-axis magnetic field	7.7 T
Ion temperature	119 keV
Electron temperature	91 keV
Electron density	$8 \times 10^{20} \text{ m}^{-3}$
Volume-averaged beta	0.6
(plasma pressure/magnetic field pressure)	
End cell lengths	6 m

considered, since steady state operation is not required. With resistive coils, the I^2R power is to some degree offset by the greater heat of vaporization of the coolant (H_2 vs. He) and reduced nuclear shield mass. The final consideration in choosing superconducting coils was the fact that superconducting coils can be kept energized in persistent mode indefinitely before startup with negligible energy expenditure by use of demountable current leads; resistive coils cannot be energized until immediately before startup because of steady-state power consumption. The combination of resistive

TABLE 4. Preliminary SOAR Reference Case Magnet Parameters

Central Cell	
Module length	3.05 m
Number of modules	24
On-axis field	7.7 T
Peak field	7.8 T
Total stored energy	6200 MJ
Winding pack inner radius	1.07 m
Winding pack thickness	62 mm
Conductor type	NbTi/Cu/Al
Cooling method	2-phase He I force-flow
Choke Coils	
Winding pack length	2.3 m
On-axis field	18.0 T
Peak field	20.2 T
Winding pack inner radius	1.0 m
Winding pack thickness	0.41 m
Conductor type	
- grades I and II	Nb ₃ Sn/Cu
- grade III	NbTi/Cu
Cooling method	Pressurized stagnant He II

central cell energy storage requirements (6200 MJ), the need for a startup power supply capable of energizing the coils in 60 s or less, and the additional power conversion equipment for supplying I^2R power during the burn make the total mass of the resistive coil option considerably larger than the superconducting option.

Various options for cooling the windings were considered. The simplest approach is cooling with stagnant pressurized superfluid helium (He II). In

all of the approaches considered, a small refrigerator/liquefier is provided to handle standby (reactor off) heat loads due to conduction and thermal radiation. Nuclear heating loads during the plasma burn are much greater and are absorbed by single-phase heating and/or vaporization of liquid helium. Nuclear heat during operation is conducted radially outward through cooling passages in the windings to a reservoir outside of the windings. The drawback to the above approach is that the specific cooling capacity available is only the enthalpy change for single-phase heating between about 1.5 and 2.0 K, namely 1.4 kJ/kg.

The remaining options, listed below, all involve evaporation of liquid helium, in order to take advantage of the enthalpy difference of about 20 kJ/kg between the liquid and vapor phases. They are:

1. Windings with boiling He I or He II and artificial gravity for phase separation;
2. Open-loop He I-cooled force-flow conductor with pumped two-phase helium;
3. Single-phase force-flow conductor with pump and evaporative heat exchanger; and
4. Pressurized He II in windings with evaporative He II heat exchanger.

Option 1 was eliminated because of complications in system design caused by spinning the entire reactor around the central cell axis in order to provide artificial gravity. Option 3 was eliminated because of the mass of a second pump and heat exchanger required; one pump is needed for the primary loop and a second for supply of the heat exchanger. In comparing the remaining two options, option 2 is preferable because a He II heat exchanger is very massive. In all of the evaporation modes considered, a high-capacity liquid

acquisition system to ensure supply of the liquid phase only to the pump is needed.

All of the evaporative modes require discharge during the 600 s of operation of large quantities (~ 80 tonnes) of cold (5 K) helium vapor into space or into auxiliary space platforms. If dumped directly into space, the resultant helium concentration is a potential problem for reactor operation because of possible electrical breakdown in the direct converter and contamination of the plasma. In order to estimate helium concentration near the reactor, an analytic solution to helium flow for the spherically symmetric, irrotational case was obtained. For a mass efflux rate of 100 kg/s, the helium concentration at a point 100 m distant from the source is about 10^{22} particles/m². These levels may be too high to be acceptable. However, preliminary estimates indicate that with directed ducting of the vapor and use of shrouds around critical system components, the above figure can be reduced by three orders of magnitude or more, i.e. to acceptable levels.

Choke Coils

The most advanced components of the magnet system are the two high-field, superconducting choke coils. The windings are cooled by He II conduction; superfluid temperature is needed because of the extremely high peak field (20.2 T) in the winding pack. In the present design, magnetic stresses are carried by graphite-epoxy composite interleaved with the conductor. The major technical problems are the relatively low transverse modulus and strength of the composite and the mismatch in thermal contraction between the composite and the Nb₃Sn/Cu conductor. Possible approaches to solving the thermal contraction problem are winding under tension in order to put the conductor under compression at room temperature or winding at low temperature. The most

satisfactory solution would be use of a composite with compatible thermal contraction behavior.

IV. MAGNET SHIELDING

SOAR requires an efficient and lightweight shield to protect the superconducting magnet against neutrons and neutron-induced gamma rays. The central cell magnets are in the highest neutron flux, and we have concentrated on designing a shield for those magnets. Many shielding, structural, and coolant materials have been evaluated to assess their neutronics performance and shielding capability. Since the central cell accounts for more than one-half of the mass of the reactor, an optimization study was performed in which the total mass of the central cell was minimized. This included the mass of the shield, superconducting magnet, and magnet He coolant. The results indicate that, for a 1000-MWe fusion reactor, the mass of the central cell amounts to 300 tonnes and this corresponds to an optimum LiH shield thickness of 0.35 m. Calculations have been done for both the 1000-MWe reference case (SOAR-1000), with a ^3He to D ratio of 1.4 to 1, and for a 250-MWe case (SOAR-250), with a ^3He to D ratio of 3 to 1.

Due to the short operation time of SOAR, the main concern is not radiation damage to the superconducting magnet but is the difficulty of nuclear heat rejection from the 4.2 K magnet. In order to lower the helium coolant mass required to remove this heat from the magnet, shields must be used to reduce the heat by several orders of magnitude. The structure and coolant constitute a small fraction of the shield volume and calculations show that they have no significant effect on magnet heating. Therefore, the choice of coolant and structure should be based on other aspects such as mechanical de-

sign, thermal hydraulics, material compatibility, strength and stress limitations. LiH was found to be the best shielding material that can meet the combined criteria of highly efficient and lightweight shield.

Many magnet shields have been designed for terrestrial fusion power reactors. However, these shield designs have emphasized economics, efficiency, and environmental considerations. As a result they include many heavy components that would not be attractive for space applications. The primary design consideration for the SOAR shield was the minimization of the overall mass of the central cell -- which includes the shield, the S/C magnet, and its cryogenic coolants. The approach followed in the design was to:

1. Assess the shielding capability of the different materials;
2. Optimize the shield thickness to minimize the central cell mass for the most promising shields; and
3. Use the results of the optimization study to select a shield type for the baseline design.

Shielding Material Selection

The choice of the shielding material was based on two considerations: the allowable radiation limits at the magnet and the neutron source energy spectrum. In general, the radiation effects in the magnet must be below certain limits in order to insure the proper performance of the magnet. For instance, the end of life dose to the epoxy insulator should not exceed 4×10^8 rads to insure the mechanical and electrical integrity of the insulator. The fast neutron fluence ($E_n > 0.1$ MeV) is limited to 10^{19} n/cm² to avoid degradation of the critical properties for the superconductor material. A low nuclear heating in the magnet is preferable to avoid excessively high cryogenic load. In addition, the neutron-induced damage to the stabilizer in-

creases the resistivity and influences the magnet stability and coil protection. In SOAR, our concern is not with radiation damage to the magnet constituents since SOAR is a low fluence machine (600 s operation time). Thus, the fluence-related radiation effects such as the dose to the insulator, the fluence to the superconductor, and the stabilizer damage do not influence the shield design. The main concern is the difficulty of nuclear heat rejection from the 4.2 K magnet. An unshielded coil is directly exposed to several tens of MW of nuclear heating. For the helium mass required to remove this heat from the magnet to be tolerable, a shield must be used to reduce the heat by several orders of magnitude. On this basis, the nuclear heating in the magnet is the driver for the shield design in SOAR.

The other factor that affects the choice of the shielding material is the neutron source spectrum. As mentioned earlier, the neutron source spectrum has two components, one at 14.1 MeV and the other at 2.45 MeV. The relative number of neutrons in each component is related to the ratio of the D and ^3He species used in the fuel cycle. For instance, 25% and 75% of the total source neutrons are D-T and D-D neutrons, respectively, for SOAR-1000 using a mix ratio of 1.4:1. The corresponding values for SOAR-250 using a mix ratio of 3:1 are 22% and 78%, indicating a slightly softer neutron spectrum. In order to attenuate such a neutron source, the shielding materials must have a good slowing down capability for energetic neutrons, and a high absorption cross section for slowed down neutrons.

Many shielding, structural, and coolant materials were evaluated to assess ability to protect the S/C magnet of the central cell. These materials are listed in Table 5. Enriched boron (90% ^{10}B) and lithium (90% ^6Li) are

TABLE 5. Materials Evaluated for the Shield

Shielding Material	Structure	Coolant
SiC	Al	H ₂ O
Pb	Ti	Li
H ₂ O	SiC	He
Ti	SS	
Li	Nb	
SS	Mo	
H ₂ O-B ₄ C		
B ₄ C		
LiH		

used. Many of these materials are used for terrestrial applications and each material has its merits and drawbacks particular to its use in space. Lithium and its compounds are mainly used for tritium breeding in D-T fusion reactors. Boron and lithium possess remarkably high neutron absorption cross sections for low energy neutrons -- a property of great importance in magnet shielding. The hydrogen compounds (like H₂O, LiH) are superior in slowing down the fast neutrons. Our calculations show that the addition of a small amount (2%) of B₄C significantly improves the neutronics performance of the water shield. LiH combines both slowing down and absorption properties in addition to being one of the lightest materials in the list. Note that Li and LiH are extensively used in space fission reactors (Barattino et al. 1985 and JPL 1985) and propulsion systems (Hyde 1983).

The neutronics performance of the shielding materials was estimated using the one-dimensional (1-D) neutron-photon transport code ONEDANT (O'Dell et al.

1982). The geometric model is shown schematically in Figure 9. The XSLIB cross section library used is derived from the ENDF/B-V evaluation. It is a 30 neutron group and 12 gamma-ray group cross section set constructed for the analysis of fusion reactor neutronics problems. The central cell of SOAR was modeled as an infinite cylinder with plasma and first wall radii of 0.60 and 0.75 m, respectively. The neutron source in the plasma was taken to be isotropic with an energy distribution in which 22% of the neutrons are at 14.1 MeV and 78% at 2.45 MeV. The D-T neutrons carry most of the energy (~ 60%) to the first wall and produce 70% of the heating in the magnet. The total neutron wall loading (from both D-T and D-D neutrons) is 0.05 MW/m^2 . These parameters pertain to SOAR-250. A direct comparison between the neutronics related parameters is made in Table 6 for the two SOAR designs. There is no essential difference neutronically between the two cases except that SOAR-1000 requires a thicker shield because of the higher wall loading and the harder neutron spectrum. Thus, the conclusions of the material selection study should be valid for SOAR-1000, as well as for SOAR-250.

Calculation of the peak nuclear heating, which occurs at the inner portion of the magnet, was made for a preliminary shield thickness of 0.15 m. The composition of the shield was taken as 80 vol% shielding material, 10 vol% structure, and 10 vol% coolant. Three sets of calculations were performed to assess the effect of the shielding material, structure, and coolant on the nuclear heating. The results are summarized in Table 7 along with the densities of the different shields. In the first set of calculations, aluminum structure and water coolant were used with the different shielding materials. As will be shown shortly, the use of other structure or coolant should not

	Thickness (cm)
Plasma	
Halo	
First Wall	1
Shield	
Clearance	1
Thermal Insulation	4
Inner Coil Case	3
S/C Coil	6.2
Outer Coil Case	3

FIGURE 9. Schematic of Central Cell Shield and Superconducting Magnet.

**TABLE 6. Neutronics-Related Parameters for the
250 and 1000 MWe Designs of SOAR**

	Medium Power	High Power
Output Power (MWe)	250	1000
Fusion Power (MW)	586	1900
Central Cell Length (m)	20	73
First Wall Radius (m)	0.75	0.63
Operating Time (s)	600	600
Neutron Wall Loading (MW/m ²)	0.05	0.24
³ He:D Ratio	3:1	1.4:1
Neutron Source Particle Percentage:		
D-D n's (at 2.45 MeV)	78%	75%
D-T n's (at 14.1 MeV)	22%	25%

alter the ranking of the shielding materials. It is clear from the table that the peak nuclear heating varies over a wide range and that a proper choice of the shielding material could result in a considerable saving in the central cell size and mass. The LiH shield produces the lowest magnet heating and has the second lowest density after the Li. In the second and third sets of calculations, the impact of using different structural materials and coolants was analyzed. As noted in the table, the nuclear heating and shield density vary only slightly. This is attributed to the small volume content of the structure and coolant in the shield. Therefore, we conclude that the structure and coolant have no significant effect on the heating in the magnet. The choice between them should not be based on the neutronics performance, but rather on other aspects such as the mechanical design, thermal hydraulics, material compatibility, strength, and stress limitations.

**TABLE 7. Effect of Shielding, Structural, and Coolant Materials
on Peak Nuclear Heating in the S/C Magnet**

	Peak Nuclear Heating (kW/m ³)	Shield Density (kg/L)
<u>Shielding Materials</u>		
SiC/H ₂ O	164	3.0
Pb/Al/H ₂ O	150	9.96
H ₂ O/Al	140	1.17
Ti/H ₂ O	135	4.15
Li/Al/H ₂ O	84	0.80
SS/H ₂ O	81	7.18
H ₂ O-B ₄ C/Al	53	1.20
B ₄ C/Al/H ₂ O	36	2.13
LiH/Al/H ₂ O	30	0.96
<u>Structural Materials</u>		
LiH/Ti/H ₂ O	31.1	1.14
LiH/Mo/H ₂ O	30.0	1.71
LiH/Al/H ₂ O	29.9	0.96
LiH/Nb/H ₂ O	29.7	1.53
LiH/SS/H ₂ O	28.9	1.48
LiH/SiC/H ₂ O	28.5	1.01
<u>Coolant Materials</u>		
LiH/Al/H ₂ O	29.9	0.96
LiH/Al/Li	31.6	0.91
LiH/Al/He	33.9	0.86

Central Cell Mass Minimization

Although the shielding material study indicates that LiH is the candidate shield, three other lightweight shielding materials were also considered. These are the Li, B₄C, and H₂O-B₄C shields. A heavy shielding material with a

good neutronics performance may lead to a thin shield and, thus, a smaller magnet. Because the magnet has the dominant mass among the central cell components, this may lead to a lower central cell mass.

The objective of the mass optimization study was to determine the shield thickness that minimizes the central cell mass -- which includes the shield, magnet and its He coolant. The study was carried out for the four shielding materials mentioned above with 5 vol% Al structure and 5 vol% He coolant. At the end, a comparison was made between the mass of the central cell components to select a shielding material for SOAR.

Knowledge of the variation of the nuclear heating in the magnet with the shield thickness was needed for the optimization study. Figure 10 demonstrates this variation and shows the decrease in the nuclear heating with the increase in the shield thickness. Note that LiH and B₄C have better attenuation for the radiation than Li or H₂O-B₄C shields. The total nuclear heating (P) in the winding pack and cases of the magnet was used to calculate the mass of the He (m_{He}) needed to cool the magnet through the relation $m_{He} = Pt/h$, where t is the operating time of the reactor, and h is the He specific heat of evaporation which amounts to 21 J/g at 4.2 K. A weight penalty factor of 2 was included to account for the container that carries the liquid He to orbit.

The masses of the central cell components along with the total mass for SOAR-250 are plotted versus shield thickness in Figure 11. By inspection of Figure 11, several general trends can be observed: as the shield thickness decreases, the He becomes the heaviest component because more nuclear heating must be removed from the magnet; the magnet has the dominant mass at the optimum point; and minimum total masses of 60, 74, 84, and 86 tonnes occur at

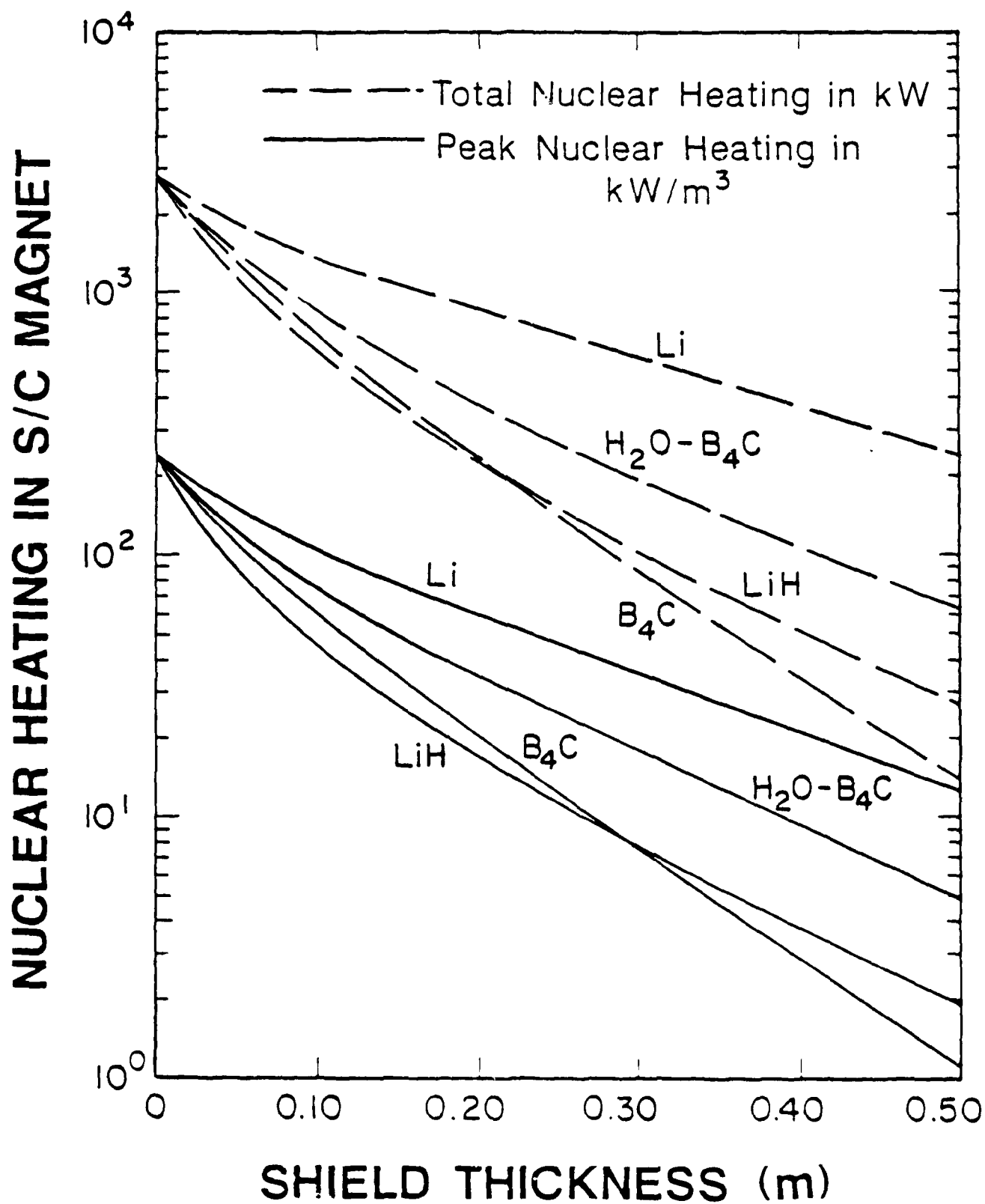


FIGURE 10. Variation of the Nuclear Heating in the Magnet with the Thickness of the Different Shields for SOAR-250.

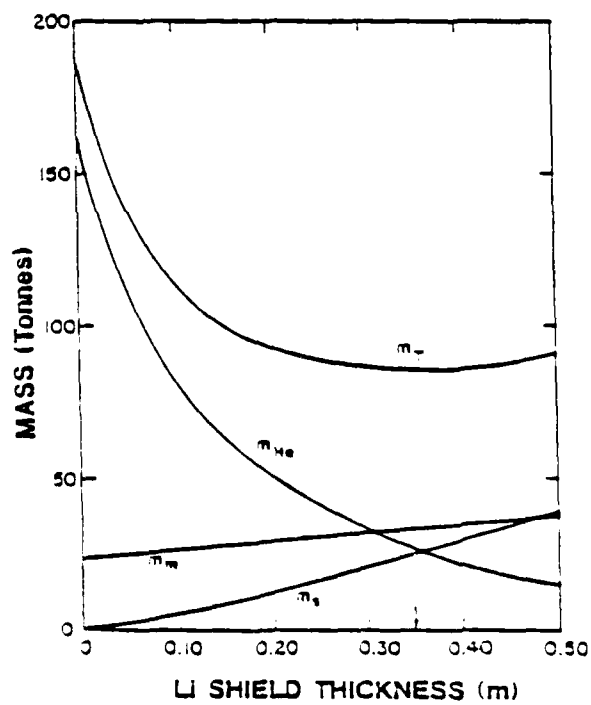
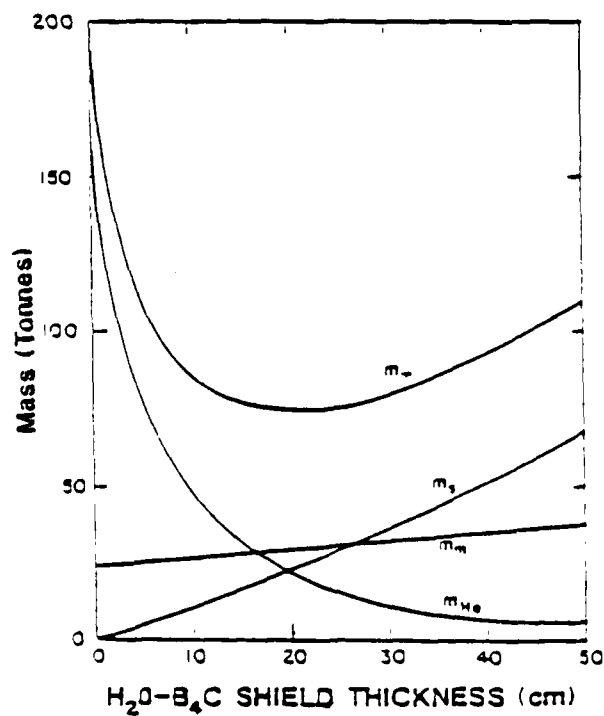
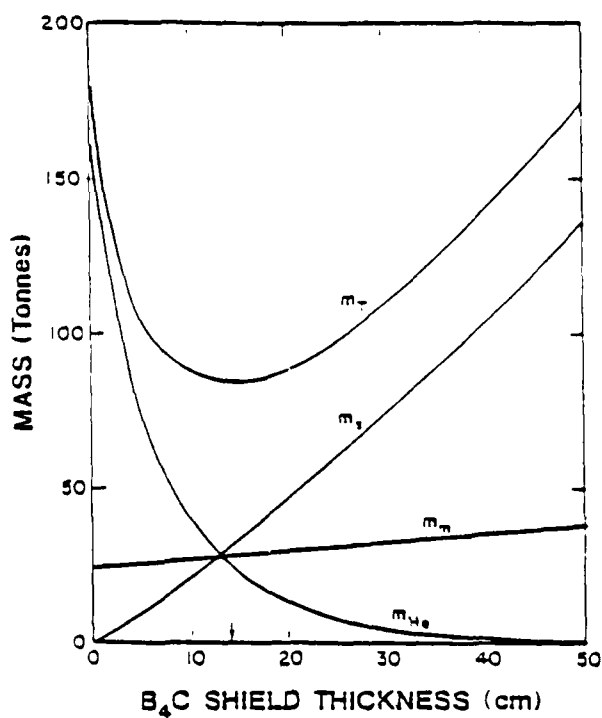
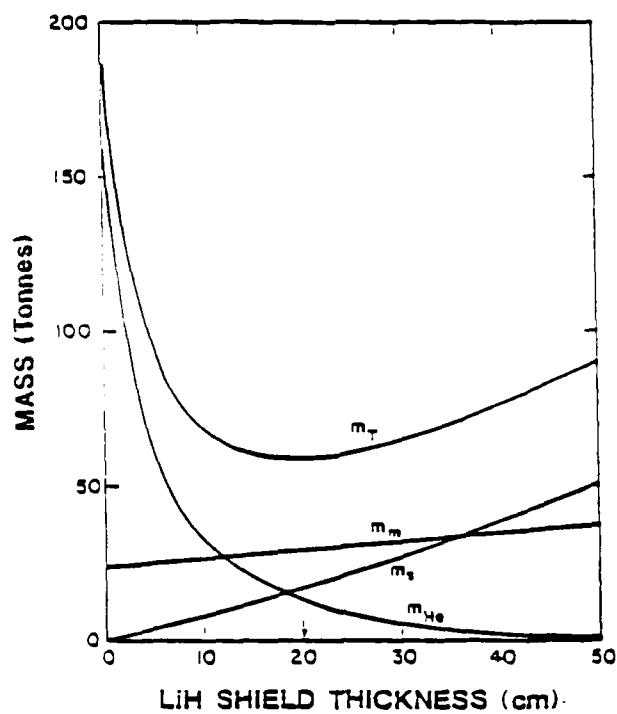


FIGURE 11. Mass of Central Cell Components as a function of the Shield Thickness for SOAR-250.

optimum LiH, H_2O-B_4C , B_4C , and Li shield thicknesses of 0.2, 0.2, 0.14, and 0.35 m, respectively. Table 8 details the central cell component masses at the optimum thickness for the four shields. Clearly, the LiH shield results in the least central cell mass. On this basis it was selected as the shield to protect the S/C magnets of SOAR.

SOAR-1000 Shield Design

The SOAR-1000 design calls for a longer central cell to produce the factor of four necessary power level. When compared to the SOAR-250 design, the neutron wall loading is a factor of ~ 5 higher. This means that a thicker shield is required to protect the S/C magnet. A similar mass optimization study was performed for the SOAR-1000 design and the results are shown in Figure 12. The minimum central cell mass is ~ 300 tonnes and this corresponds to an optimum LiH shield thickness of 0.35 m. Other data of interest are the peak nuclear heating and the inner bore radius of the magnet. These are 23 kW/m^3 and 1.04 m, respectively. Similarly, the total mass for the shield, magnets, and He coolant in the end cells is ~ 100 tonnes.

V. HEAT DISSIPATION IN THE SOAR REACTOR

Heat dissipation in space has always been a challenging problem and continues to be a major subject for investigators. Basically, there are two ways to manage heat in space; the first is to radiate it away and the second is to absorb it adiabatically during the burn. Heat dissipation by radiation is the most commonly used method in space and is the only viable method for long term steady-state dissipation. It takes the form of rather bulky and heavy radiators which are vulnerable to meteoroid damage, as well as more innovative but

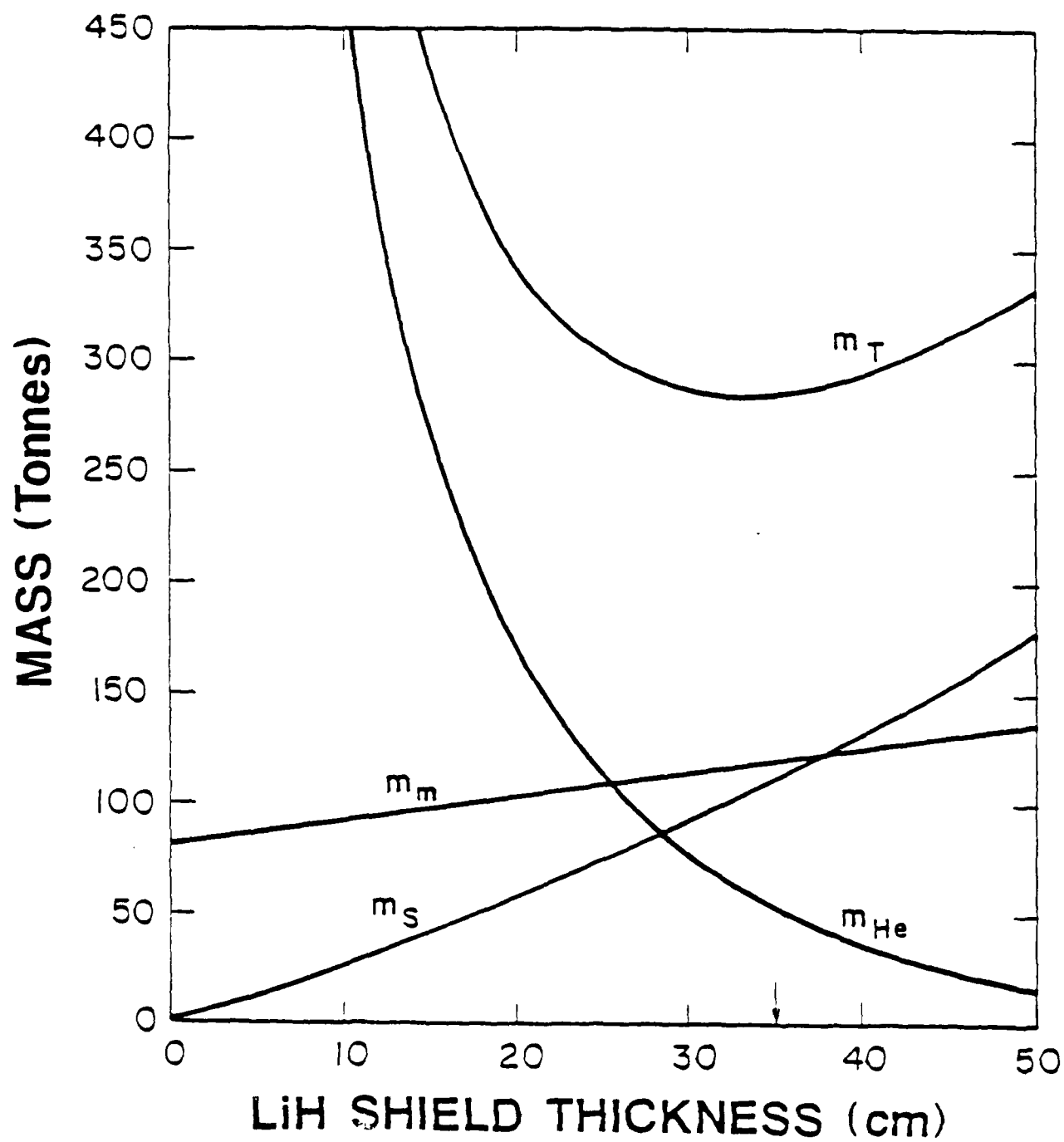


FIGURE 12. Mass of Central Cell Components as a function of the LiH Shield Thickness for SOAR-1000.

TABLE 8. Comparison between the Masses of the Center Cell Components
for the Four Shields

Shield Type	Optimum Shield	Shield	Peak Nuclear	$IR_{S/C}$ (m)	m_S (tonnes)	$m_{S/C}$ (tonnes)	m_{He} (tonnes)	m_T (tonnes)
	Thickness (m)	Density (kg/L)	Heating (kW/m ³)					
Li	0.35	0.62	27	1.19	25	34	27	86
B ₄ C	0.14	2.1	36	0.98	31	28	25	84
H ₂ O-B ₄ C	0.20	1.1	20	1.04	23	30	21	74
LiH	0.20	0.8	17	1.04	17	30	13	60

unproven schemes such as dust column, liquid droplet, and liquid belt radiators. Adiabatic heatup is only viable for systems, such as SOAR, with a short term burst mode of operation. The shield materials presently considered for SOAR, LiH and Li, also have the requisite characteristic needed for adiabatic heatup, namely a high specific heat. Additionally, they are of low density, have a low vapor pressure, are stable, are compatible with structural materials, and undergo a phase change which can be put to advantage for absorbing heat. These materials can, therefore, double as shields and as heat absorbers. Table 9 gives the pertinent thermal and physical properties of LiH and Li.

The D-³He reaction produces a very high ($\sim 1.6 \text{ MW/m}^2$) surface heat load on the first wall, and this heat must be diffused throughout the shield for this scheme to work. Unfortunately, no material has a high enough thermal conductivity to be able to do this in 600 s without exceeding the melting

**TABLE 9. Pertinent Properties of LiH and Li for the
Shield Adiabatic Heatup Calculations**

	Temp. (K)	LiH	Li
Specific heat (kJ/kg K)	200-300	3.75	2.9
	300-500	4.60	3.9
	500-800	6.05	4.3
Melting temp. (K)		960	453
Heat of fusion (kJ/kg)		2770	433
Thermal conductivity (W/mK)	470	4.4	44
	620	4.1	47
Vapor pressure (torr)	900	6.7×10^{-2}	7.6×10^{-2}
Density (kg/m ³)	solid	780	530
	liquid	550	520

temperature of the first wall. The heat distribution method we have adopted is a circulating He gas which uses the first wall as a heat source and the bulk shield as the sink. Thus, the first wall consists of a bank of tubes through which the He gas flows and absorbs the surface heat. From there the gas circulates through the shield in tubes immersed in the shielding material. Figure 13 shows a section of the central cell with the plasma in the center, surrounded by the shield and the magnet. The arrows show the flow distribution of the He gas. Gas circulators are strategically located along the central cell with the motors outside the magnet. Figure 14 gives the dependence of the average shield temperature on time for the SOAR reference case shield.

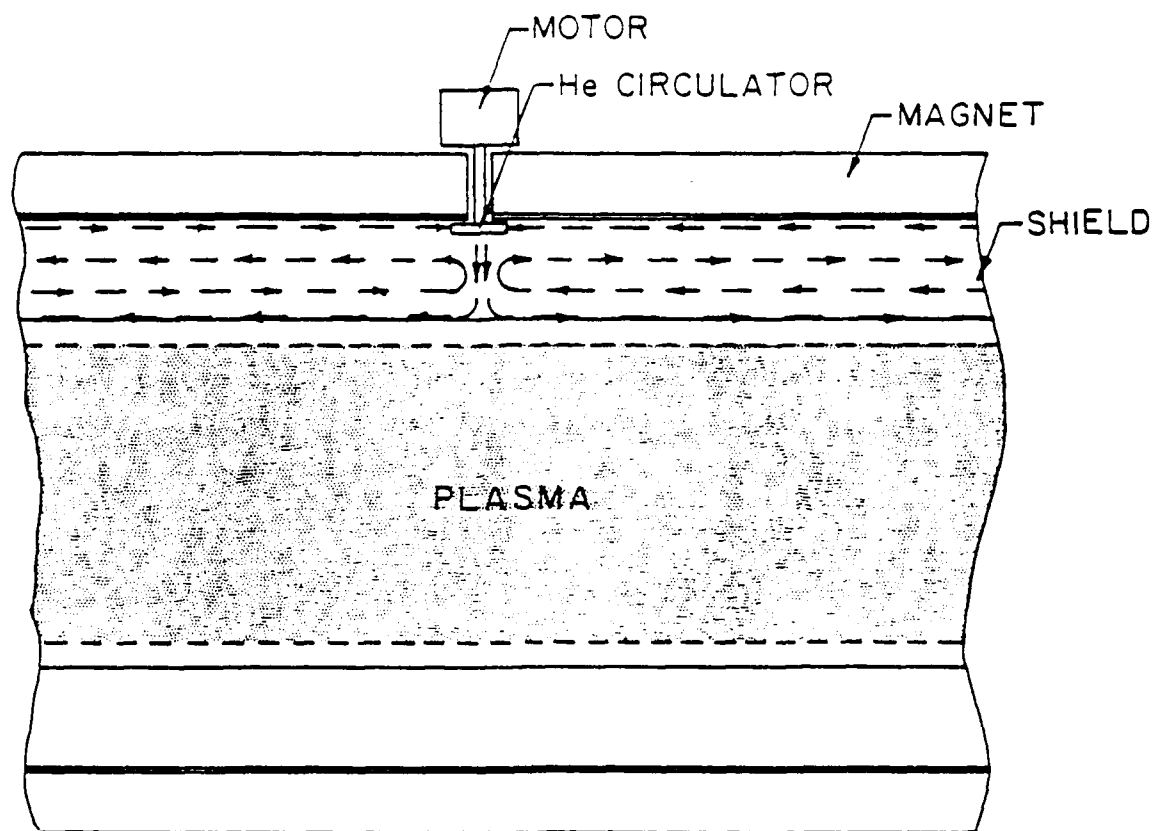


FIGURE 13. A Section of the Central Cell with the Plasma in the Center, Surrounded by the Shield and the Magnet. Arrows Show the Flow Distribution of the He Gas.

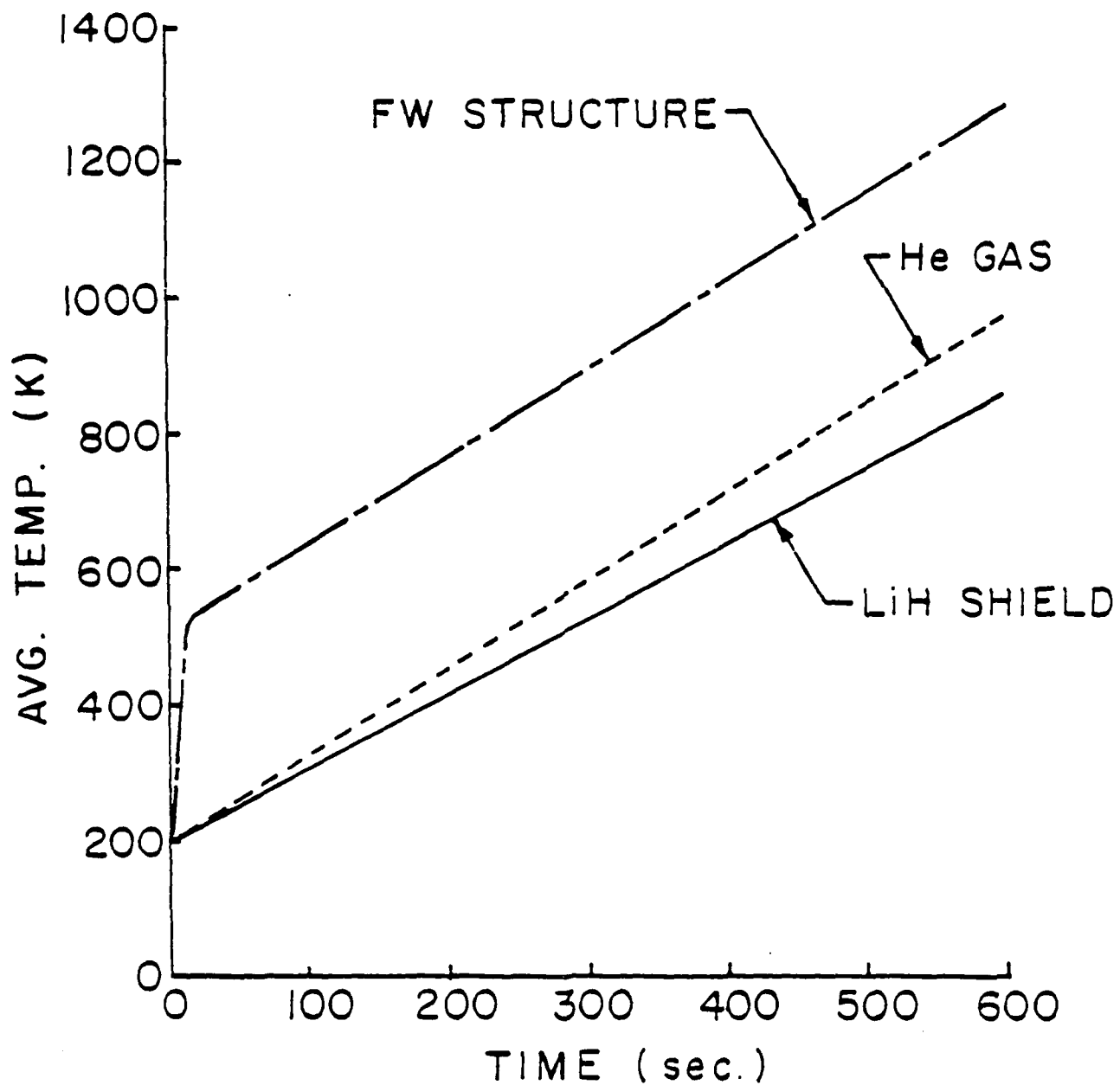


FIGURE 14. Average Temperature of the SOAR Shield as a Function of Time.

LiH is the best shield from the standpoint of minimization of mass. The melting temperature of LiH is 960 K and its heat of fusion is 2770 kJ/kg. Its primary drawbacks are a low thermal conductivity and a high expansion upon melting. The best way to use it would be below the melting point. However, it will be very difficult to prevent melting at some localized hot spots. The two primary structural material candidates are Mo and Nb alloys with a slight preference for the Nb alloy. Both have high strength at elevated temperatures up to ~ 1600 K and have a low thermal stress coefficient, as shown in Figures 15 and 16. The Nb alloy, however, is more easily fabricated and is much more ductile over the whole operating temperature range.

In summary, an adiabatic heatup shield can be designed for SOAR, using LiH as the primary shield material, Nb alloy as the structure and circulating He gas as a means of distributing the heat. The burn is assumed to last for 600 s and the ambient temperature to be 200 K. The average temperature of the shield reaches 808 K, well below its melting point.

VI. DIRECT CONVERTER

An electrostatic direct converter is used at one end of SOAR to convert the directed kinetic energy of particles streaming out the end of the reactor into high voltage DC power. By careful control of the mirror ratio at the two ends of the central cell and of the electrostatic potential in the two end plugs, most of the ion end loss can be directed out one end of the reactor. The electrons are directed out the other end by biasing the opposite end wall slightly positive relative to the ground potential at the entrance to the direct converter.

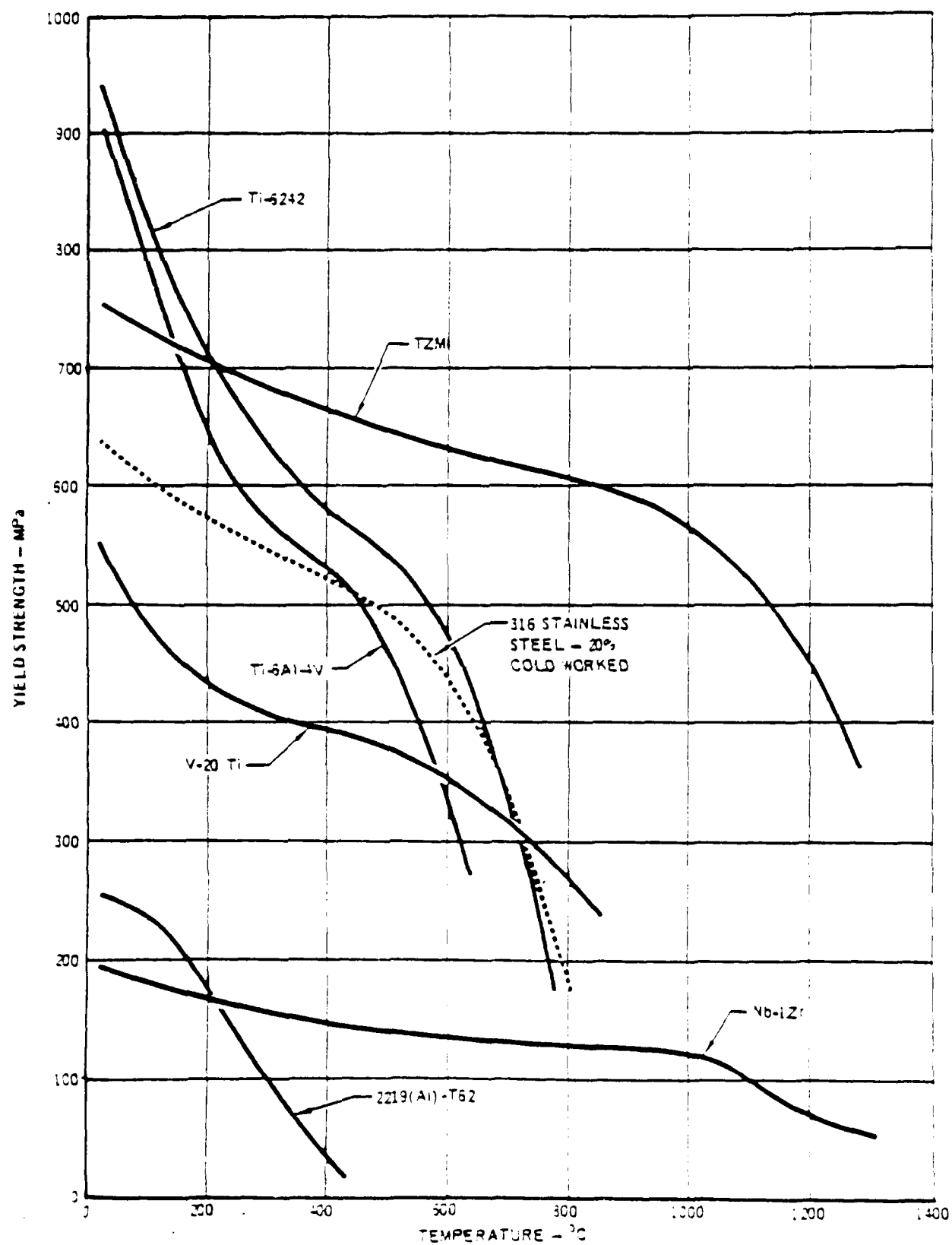


FIGURE 15. Effect of Temperature on the Yield Strength of Several Candidate materials.

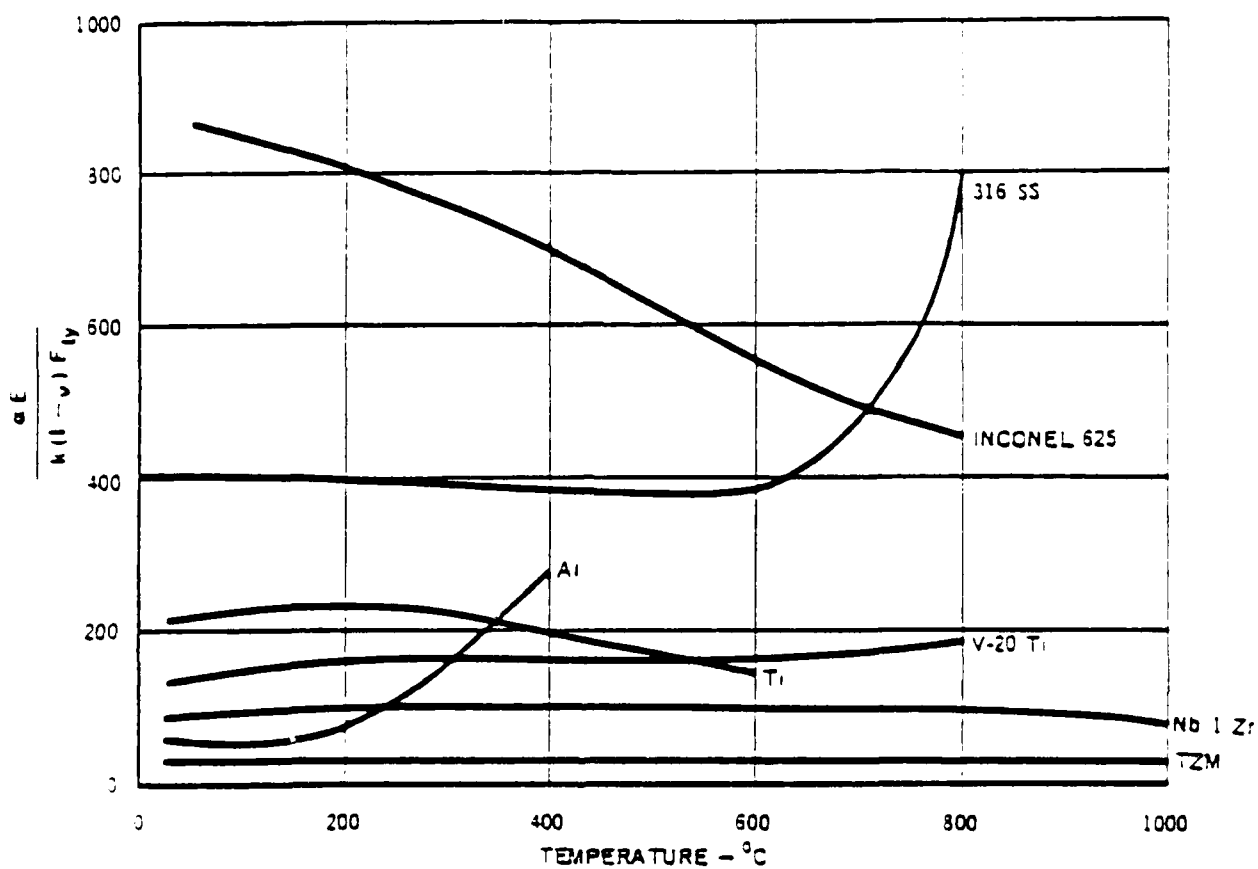


FIGURE 16. Ratio of Thermal Stress to Yield Strength for Selected Candidate Materials.

The current and power of the various energy groups of ions entering the direct converter for the reference case are shown in Table 10. The 15.2 MeV protons are those protons which were born at 14.7 MeV and scattered nonadiabatically into the loss-cone before slowing down. They acquired an additional 0.5 MeV energy because of the positive potential of the central cell. The lower energy components consist of the end loss of fuel ions, fusion-born alpha particles, and thermalized protons. Because of the energy spectrum, a "venetian blind" direct converter (Moir and Barr 1973, Barr and Moir 1983) with at least two or three-stages is desirable to achieve high efficiency. In this paper, we present results from a preliminary study of a two-stage direct converter; a three-stage direct converter is also being considered.

The SOAR two-stage direct converter collects the energetic protons at high voltage (13 MV) and the other groups at lower voltage (1.3 MV). A schematic of a two-stage converter is shown in Figure 17. The entrance grid sets the ground potential; the electron suppressor grid repels any electrons entering the direct converter so they do not get accelerated to 13 MeV and degrade the net collected current. The grids will be heated because they intercept a fraction of the incident ion flux.

Six cooling concepts were examined for the suppressor grid. The lightest mass concept was chosen for the baseline design. The first employs liquid-cooled swirl tubes where the water is discarded during power generation. In swirl tubes the water is forced to flow in a helical pattern through a circular tube. The mechanism of surface boiling with bubble recondensation in the subcooled liquid near the tube center results in an extremely high heat transfer device. In calculating the mass only the water was considered. The

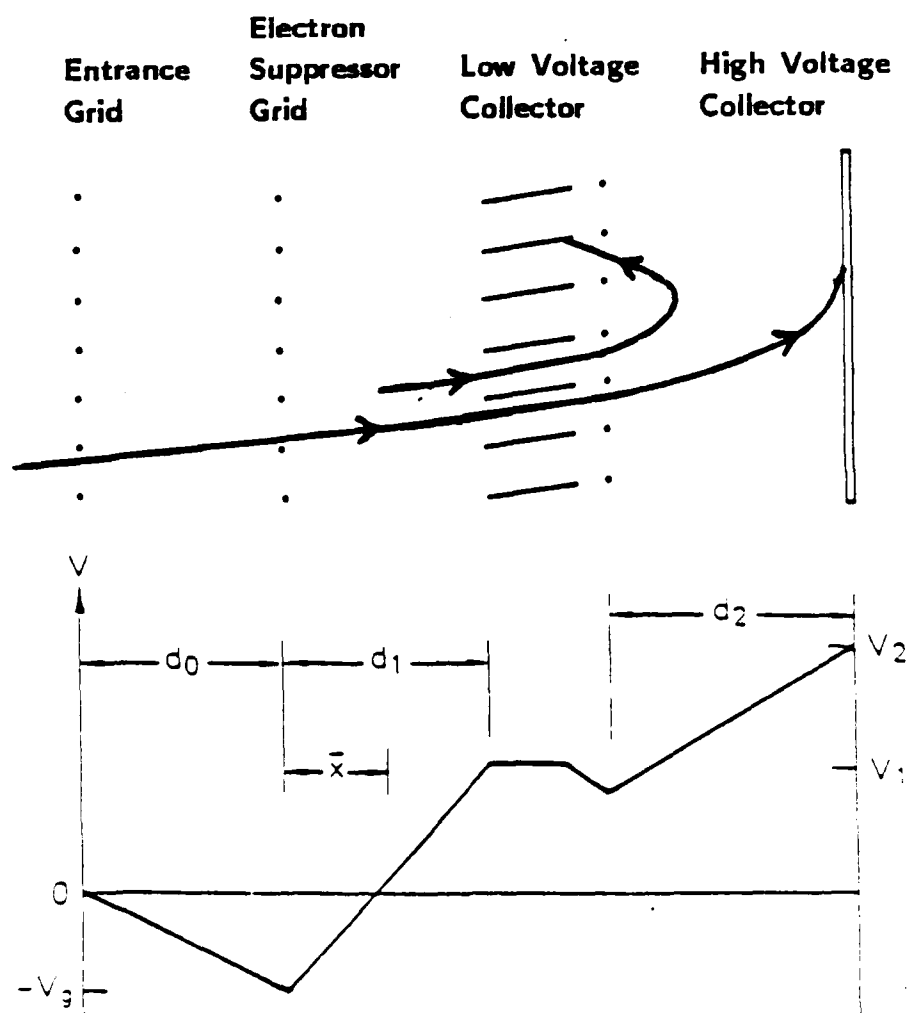


FIGURE 17. Schematic of a 2-Stage Direct Converter.

TABLE 10. Energy Spectrum Entering Direct Converter

	Species	Current (A)	Energy per Charge (MeV)	Power (MW)
High voltage	p	68	15.2	1039
Low voltage	d	1.2	3.1	4
	α	4.0	2.6	4
	d	134	1.4	142
	p	22	1.4	31
	^3He	6.3	1.4	9
	α	0.2	1.4	0.3
	e	46	0.2	9
		235 A of ions		1288 MW of ions

second concept employs swirl tubes with cooled and recirculating water. In this concept only the weight of the coolant water radiator is considered. Radiation from the radiator surface at the relatively low coolant temperature is the dominant heat conductance used to calculate the required heat transfer surface area and hence the weight of the radiator. The third concept employs forced circulation boiling liquid heat transfer. The water is recirculated through a radiator. The required radiator surface area is large due to the poor steam condensation heat conductance. Only the mass of the radiator is considered. The fourth concept employs high pressure and velocity recirculating gaseous coolant. The pressure is 140 atmospheres. Radiation from the radiator determines its size. Only the mass of the radiator is considered. The fifth concept employs the melting, during power generation, of a solid

lithium mass contained within the grid tubes. Only the mass of the lithium is considered. The sixth concept employs direct radiation from the grid element itself, and three materials were considered. The mass is that of the grid element. Table 11 shows the six concepts and their masses. The lightest mass concept is the last, the radiating grid, and it was chosen for the baseline design. Since only a part of the system mass of the other concepts was considered, their actual masses will be greater than that shown.

Three radiative grid materials were considered, carbon, TZM, and tantalum. Carbon is in the form of a carbon-carbon composite. TZM is a molybdenum alloy containing small amounts of titanium and zirconium. The carbon grid diameter is 10 mm and the TZM and tantalum grid diameters are 3 mm. The power into the direct converter is 1288 MW. Table 12 shows the suppressor grid diameter and mass for the three grid materials radiating between 1400 and 2000 C. Also shown is the thermionic emission current and the power loss. The grid diameter is determined from the heat flux for the material and radiating temperature and the power load onto the grid. The thermionic emission current is determined for the grid material and its radiation temperature. The power loss occurs because the emitted electron current flows from the grids to the high voltage collector and reduces the net collected current. The two factors in the choice of a radiating grid are the mass and power loss. Table 12 shows that the carbon grid at 1400 C has the lowest thermionic current and a mass of 3.2 tonnes. The carbon grid at 1600 C has a slightly lower mass, but the thermionic current is excessive. The carbon suppressor grid at 1400 C with a diameter of 65.5 m and mass of 3.2 tonnes, respectively, is chosen for the baseline design. Sputtering of the carbon grid during the power cycle time is negligible.

**TABLE 11. The Six Direct Converter Suppressor Grid
Cooling Concepts and Their Masses**

<u>Concept</u>	<u>Mass (tonnes)</u>
1. Surface boiling swirl tubes -- discard water	1540
2. Swirl tubes	670
3. Forced circulation boiling liquid coolant radiative heat rejection	2×10^6
4. Gaseous coolant radiative heat rejection	86
5. Solid lithium melting	89
6. Radiative grid	3.2

**TABLE 12. Suppressor Grid Diameter and Mass for the Three Grid
Materials Radiating between 1400 and 2000 C**

<u>Material</u>	<u>Grid Temp. (C)</u>	<u>Diameter (m)</u>	<u>Mass (tonnes)</u>	<u>Thermionic Emission Current (A)</u>
Carbon	1400	65.5	3.2	24
	1600	52	2.0	370
TZM	1400	122	34	47
	1800	79	14	11400
	2000	66	10	84000
Tantalum	1400	113	25	470
	1800	74	11	71000
	2000	61	7	437000

The ion collectors are designed of lightweight tantalum foil supported by a structural frame that is shielded from the ion flow. The foil is 0.13 mm thick. Tantalum foil as low as 8 μm is commercially available. The diameter of the collectors is assumed to be the same as the suppressor grid. Sputtering of the tantalum foil during the power cycle time is negligible. Table 13 shows the masses of the grids, collectors, and structural supports for the ion end of the reactor. In addition to thermionic emission, other loss mechanisms include secondary electron emission, finite opacity of the grids and low voltage collector, ion-neutral scattering in the direct converter, and the finite kinetic energy at which ions strike the collectors. The high voltage collector receives 52 A of current and 689 MW of power. The low voltage collector gathers 174 A and 226 MW. The electron suppressor grid receives 9 A and 5 MW. The net power output for the 1000 MW (nominal) case is estimated to be 910 MW, which gives an overall direct converter efficiency of 71%. This is based on a grid transparency of 99% and a "venetian blind" transparency of 95%. The lower transparency of the "venetian blinds" arises from the finite angular spread of the incident ions. A 3 stage direct converter in which the high energy protons are collected at two voltages might achieve a somewhat higher efficiency. The plasma parameter optimization assumes an overall direct converter efficiency of 78%. This value depends strongly on the energy spread of the nonadiabatic proton loss stream -- a quantity which is presently being calculated.

**TABLE 13. Masses of the Grids, Collectors, and Structural Supports
for the Ion End Direct Converter of SOAR**

<u>Component</u>	<u>Mass (tonnes)</u>
Entrance grid	3.2
Suppressor grid	3.2
Low voltage collector	7.1
High voltage collector	7.1
Structural supports	5
TOTAL	25.4

VII. POWER HANDLING

The high voltage electrical energy from the direct converter must be converted to levels suitable for distribution and for powering equipment. The detailed load requirements for SOAR have not yet been defined, and the possibility of using this energy at megavolt levels is under consideration. If the power must be used at lower voltages, several options exist.

A belt or chain driven electrostatic particle accelerator may be made to operate in the reverse mode, i.e. rather than drive the chain to carry charge to the terminal, the charge on the terminal may be used to drive the chain and thus power a conventional generator. There are two problems related to applying this approach to the present design. The first problem is that present chain design is such that only small currents may be carried by the chain. To use this technique would require an increase in current carrying capacity of between 4 and 5 orders of magnitude. The second problem, which may be of concern for any concept, is the difficulty of holding 13 MV in a vacuum. To stand off voltages this high outside the terminal in the region of the charg-

ing chain, the space between the terminal and the tank is filled with SF_6 at about 5×10^5 Pa pressure. To prevent arcing inside the accelerating column, which is in vacuum, a set of corona rings is established to carefully control the potential gradient and thus avoid gross breakdown and arcing. Since the causes and factors affecting this kind of breakdown in vacuum are not understood, an experiment and analytical study will be required.

Another technique in present use for the conversion of high voltage DC uses inverters based on switched thyristors. Since any alternating current system will require transformers and the attendant mass of the transformer core, to keep the system mass as low as possible the frequency of the system would be kept as high as possible -- no less than 400 Hz and possibly greater than 1000 Hz. The present status of thyristor development limits the voltage across one thyristor to about 5 kV. Since all of these inverting units are in series, any failure in switching one of them could result in the full 14 MV appearing across one inverter. Thus the inverting units must be carefully matched and a protection scheme devised to prevent catastrophic failure in the event of a momentary fault. Since it may not be feasible to connect the inverters as one large series unit producing 13 MV AC to be reduced to a lower voltage via transformers, the inverting units would be connected in a series-parallel fashion to provide several sources of alternating current at 200-300 kV. These sources could be coupled together via transformers to form the main power output. However, since the inverter sections run as high as 13 MV, the primary-to-secondary insulation on the transformers must withstand the voltage. This might be avoided by using each inverter to drive a motor-generator set. In this case the motor-generator shaft could be used to stand

off the voltage. The complication would be the added mass and complexity of a rotating system.

Until load requirements are specified, our primary emphasis is on collecting the power at high voltage. Nevertheless, various aspects of the power handling system are under investigation. These areas include: feasibility of improving thyristor performance, system mass, system efficiency and rejection of waste heat, network stability, ability of the source to follow the load and, failure modes and consequences. At the present time some variant of the solid state inverter scheme seems to be the choice to pursue for further investigation. However, it is possible that other more promising techniques may be found.

VIII. CONCLUSIONS

We have identified an attractive power station option for space burst mode power: the SOAR D-³He tandem mirror fusion reactor. The symbiosis of burst mode requirements, D-³He fusion reactor characteristics, and the space environment has led to large improvements over earthbound fusion reactor concepts. In particular, a mass utilization of ~ 2 kWe/kg-orbited is attained, radioactivity is absent at launch, and fuel costs are small. Key features of SOAR include the use of D-³He neutron-lean fuel, blow-through magnet cooling, and direct converters. The technology extrapolation required for SOAR appears to be reasonable, and the plasma analysis has led to plausible parameters. The mass utilization of SOAR is very attractive for space applications.

ACKNOWLEDGMENT

The authors wish to acknowledge helpful discussions with Dr. Jerry Parmer of General Dynamics.

REFERENCES

- Baldwin, D.E. and B.G. Logan (1979) "Improved Tandem Mirror Fusion Reactor," Phys. Rev. Lett. 43, 1318.
- Barattino, W.J., M.S. El-Genk, and S.S. Voss (1985) "Review of Previous Shield Analysis for Space Reactors," in Space Nuclear Power Systems 1984, M.S. El-Genk and M.D. Hoover eds., Orbit Book Co., Malabar, FL, Vol. 2, pp. 329-339.
- Barr, W.L. and R.W. Moir (1983) "Test Results on Plasma Direct Converters," Nucl. Technol./Fusion 3, 98.
- Berk, H. et al. (1984) "Stabilization of an Axisymmetric Tandem Mirror Cell by a Hot Plasma Component," Phys. Fluids 27, 2705.
- Dawson, J.M. (1981) "Advanced Fusion Reactors," in Fusion, Vol. 1, Part B, E. Teller ed., Academic Press, New York.
- El-Guebaly, L.A. (1987) "Magnet Shielding Analysis for SOAR -- A Space Reactor," in Proceedings of the 4th Symposium of Space Nuclear Power Systems, held in Albuquerque, NM, 12-16 January 1987.
- Englert, G.W. (1962) "Study of Thermonuclear Propulsion Using Superconducting Magnets," in N.W. Mather and G.W. Sutton, eds., Engineering Aspects of Magnetohydrodynamics: Proceedings, Third Symposium, Gordon and Breach, NY.
- Gurol, H., G.W. Shuy, and A.E. Dabiri (1983) "Preliminary Analysis of a Carbon/Carbon Fiber Composite Plasma Direct Converter," Nucl. Technol./Fusion 4, 1473.
- Hershkowitz, N. et al. (1985) "Plasma Potential Control and MHD Stability Experiments in the Phaedrus Tandem Mirror," Tenth International Conference on Plasma Physics and Controlled Nuclear Fusion Research, IAEA, Vienna.
- Hilton, J.L., J.S. Luce, and A.S. Thompson, "Hypothetical Fusion Propulsion Rocket Vehicle," J. Spacecraft 1, 276.
- Hyde, R.A. (1983), "A Laser Fusion Rocket for Interplanetary Propulsion," UCRL-88857, Lawrence Livermore National Laboratory, Livermore, CA.
- JPL (1985), "SP-100 Ground Engineering System Baseline System Definition and Characterization Study, Final Report Vol. I," General Electric Company, Philadelphia, PA, 9 August 1985.
- Kesner, J. et al. (1984), "Introduction to Tandem Mirror Physics," PFC/RR-83-35, Massachusetts Institute of Technology, Cambridge, MA.
- Kesner, J. et al. (1985), "Axisymmetric Tandem Mirror Stabilized by a Magnetic Limiter," PFC/CP-85-5, Massachusetts Institute of Technology, Cambridge, MA.

- Logan, B.G. et al. (1984), "Mirror Advanced Reactor Study," UCRL-53480, Lawrence Livermore National Laboratory, Livermore, CA.
- Logan, B.G. et al. (1986), "MINIMARS Conceptual Design Final Report, Vols. I and II," UCID-20773, Lawrence Livermore National Laboratory, Livermore, CA.
- Miley, G.H. (1976) Fusion Energy Conversion, American Nuclear Society, La Grange Park, IL.
- Moir, R.W. and W.L. Barr (1973) "'Venetian Blind' Direct Energy Converter for Fusion Reactors," Nucl. Fusion 13, 35.
- O'Dell, R.D. et al. (1982), "User's Manual for ONEDANT: A Code Package for One-Dimensional, Diffusion-Accelerated, Neutral Particle Transport," LA-9184-M, Los Alamos National Laboratory, Los Alamos, NM, February 1982.
- Santarius, J.F. et al. (1987a) "SOAR: Space Orbiting Advanced Fusion Power Reactor," in Trans. 4th Symposium on Space Nuclear Power Systems, CONF-870102-Summs, held in Albuquerque, NM, 12-16 January 1987.
- Santarius, J.F. (1987b) "Very High Efficiency Fusion Reactor Concept," Nucl. Fusion 27, 167.
- Wittenberg, L.J., J.F. Santarius, and G.L. Kulcinski (1986) "Lunar Source of ^3He for Commercial Fusion Power," Fusion Technol. 10, 167.
- Wittenberg, L.J., J.F. Santarius, and G.L. Kulcinski (1987) "Helium-3 Fusion Fuel Resources for Space Power," in Trans. 4th Symposium on Space Nuclear Power Systems, held in Albuquerque, NM, 12-14 January 1987.

END
DATE
FILMED
MARCH
1988
DTIC